BABEȘ-BOLYAI UNIVERSITY CLUJ-NAPOCA   FACULTY OF PHYSICS

SERS applications - from molecules to microorganisms

Nicoleta Elena Mircescu

PhD Thesis Summary

Scientific supervisor: Prof. Dr. Vasile Chiș

Cluj-Napoca

2013

Contents

Introduction

The present doctoral thesis work aims to improve of pre-existing analytical methods as well as to develop innovative procedures for the identification of (bio) molecules of interest, with special attention being devoted to **Surface-enhanced Raman scattering (SERS)**. The scientific results here reported are the fruit of a research activity carried out both at "Babeş-Bolyai University" Cluj-Napoca, under the guidance of Prof. Dr. Vasile Chiş and Prof. associated Dr. Nicolae Leopold and at Technische Universität München (TUM) in collaboration with PD Dr. Christoph Haisch and Dr. Natalia P. Ivleva, respectively.

Firstly, the **state of the art** is introduced to the readers. The introduction part is limited to the motivation of employing a synergistic theoretical and spectroscopic tool in the detection of the selected compounds and microorganisms. The importance of the scientific work is highlighted and a wide research background is reported, in order to underline the innovative approach of this original thesis.

The second section of the thesis introduces the theory background on which relies the processing and interpretation of the information obtained by **Density Functional Theory (DFT)** calculations. It also describes the spectroscopic methods used for the experimental investigation of the compounds. The following three chapters are considered to illustrate the applications of the mainly dedicated method, SERS, and points out the useful information that is provided by vibrational spectroscopy.

In **Chapter 3** nitrogen-rich molecular compounds were studied by using the remarkable sensitivity of SERS coupled with other spectroscopic methods and the excellent accuracy of the DFT calculation. Vibrational **Fourier transform infrared spectroscopy (FTIR)**, **Raman** and **SERS** spectra of melamine and zidovudine were successfully recorded in aqueous solutions and the specific wavenumbers were assigned based on B3LYP/6-31G(d) or B3LYP/6-311++G(d,p) quantum chemical calculations and discussed in order to determine the adsorption geometry of these molecules on silver colloidal surfaces. The adsorption geometries of these two compounds are deduced by calculating the 3D molecular electrostatic potential surfaces.

The fourth section is dedicated to the synthesis of new SERS-active substrates, including an in-situ laser-induced silver substrate and a novel, green and simple synthesis of highly biocompatible gold **nanoparticles (NPs)** by using polymers as reducing agent.

In **the last chapter**, the results obtained in the 6 months internship at TUM focused on the SERS detection of **Urinary Tract Infections (UTIs)** causative pathogens are reported. The aims of this study are the discrimination of rough and smooth *E. coli* strains and the receptor-free SERS detection of two most common uropathogens (*E. coli* and *P. mirabilis*).

Research background

Medical physics and biophysics contribute to maintaining and improving the quality, safety and cost-effectiveness of healthcare services by means of oriented activities requiring expert evaluation, monitoring and measurements of specific and selective parameters. The field includes ionising and non-ionising electromagnetic radiations, static electric and magnetic fields, ultrasound, laser light and other assessments associated with medical devices.

Currently, in literature, the most common methods for detection at trace level of the compounds of medical or pharmacological relevance are **high performance liquid chromatography (HPLC)** or more recently, in order to study their *in vivo* bioavailability and bioequivalence, the **micellar liquid chromatography (MLC)** [1-4]. One of the adulterants for feedstock and milk, used mostly in China for several years is the nitrogen-rich compound 1,3,5-triazine-2,4,6-triamine, or **melamine**. Melamine and its analogues are used in food processing to fraud the products which are tested for their protein content, threading the health of the consumers. Conventional methods as HPLC, **liquid chromatography (LC)**, TLC, **liquid chromatography - mass spectrometry (LC-MS)** cannot satisfy the need in practice being time-consuming (the milk gets spoiled and must be assayed within 4 h). For this reason, reliable detection and qualification of melamine residues and other potentially toxic contaminants in food represents a very important safety issue, the proficiency of several laboratories to determine melamine in food being recently assessed [5]. The reason why melamine is toxic even in small amounts (the maximum amount allowed in powdered infant formula is **1mg/kg** and in other foods is **2.5mg/kg**) lays on its interaction with cyanuric acid by hydrogen bounds in order to form a crystalline complex that turns into an insoluble precipitate in kidney tubules when co-ingested [6].

The detection of **melamine** by using Raman spectroscopy in feed or in milk powder provides a limit of detection (LOD) of 10 mg/ml, which needs improvement. Another approach would be to correlate the Raman results with standard HPLC for verifying the detection accuracy [7]. In this case, the sample preparation protocol includes acetonitrile extraction of **melamine**, ultrasonication, centrifugation, dilution and then filtration of the supernatant, and finally, the **melamine** detection. This complex methodology requires more than 3 h analysis time, unacceptable for routine measurements in spiked foods. Noteworthy, the detection limits were in all tested products less than the maximum amount permitted: 1 mg/ml in wheat gluten, 0.5 mg/ml in chicken feed, 0.5 mg/ml in cakes, and 0.7 mg/ml in noodle. SERS was also proposed as detection method by other research groups [8-11]. By using SERS detection at 785 nm, 1064 nm and 1550 nm, Huang et al. [8] reached a LOD of 0.5 μg/ml in methanol value. The reported detection limits of only 0.5 mg/ml in the first study and 0.5 μg/ml respectively are due to the near-infrared (NIR) 785 nm chosen laser line. Taking in consideration the plasmon resonance of gold, and that of silver, a HeNe laser at 633 nm would be more appropriate. Zhang et al. detected melamine in liquid milk with a LOD of 0.05 µg/ml and 0.01 µg/ml for

melamine standard samples, respectively [12]. Using a "sandwich" structure SERS-active substrate, Zhang et al., detected melamine down to ppm level [13]. The aim of our investigation is to provide complementary to the analytical reports concerning melamine SERS detection, a physico-chemical characterization of both, neutral and protonated melamine molecular species, by using FTIR, FT-Raman and SERS spectroscopy, as well as theoretical calculations. The excitation laser line used by our setup is the **neodymium doped yttrium aluminum garnet (Nd:YAG)** laser with emission at 532 nm [14].

Another nitrogen-rich molecule of pharmacological relevance is **zidovudine**, or **AZT**, which acts as nucleoside reverse transcriptase inhibitor and delays the development of **acquired immunodeficiency syndrome (AIDS)** in patients infected with **human immunodeficiency virus** infection **(HIV)**. AZT is also used as a new radiosensitiser in cancer radiotherapy [15]. The characterization of this compound is important due to its worldwide usage as cytostatic antiviral drug in AIDS and cancer treatment. The detection of zidovudine (AZT) by using Raman spectroscopy was assessed in the last decades, either by excitation with the 1064 nm laser line [16], either with the 488 nm Ar^+ laser [17]. These studies aim to explain the adsorption mechanism of AZT on the silver surface or to characterize the orientation of AZT in a biological system. To the best of our knowledge, there are no vibrational studies including the AZT SERS spectrum excited with the 532 nm laser line. This work presents a SERS and DFT study on neutral and deprotonated molecular forms of zidovudine, including also its adsorption geometry on the silver surface deduced based on the molecular electrostatic potential (MEP) and the selective Raman bands [18].

A joint theoretical and experimental study was performed for each of the above mentioned nitrogen-rich compounds selected due to their biomedical relevance. The scarce vibrational studies published on **zidovudine** [1, 16-17, 19-20] and the main focus on the IR and Raman spectral features [8] are justifying this investigation by means of ultrasensitive spectroscopy. There are few DFT calculations reported on **zidovudine** [20-21] and **melamine** [22-25]. However, these studies were performed by using semiempirical [21] or post Hartree-Fock [25] theoretical methods and they don't include the vibrational frequencies calculations, being focused on the physical or electronic properties. There is one SERS-based detection of AZT study [16] in which the adsorption on a silver surface is also discussed, but no DFT study to sustain the proposed mechanism of adsorption is included. In **melamine**'s case, SERS studies reported recently are numerous [9-11, 13, 26-32]. Zhang et al. [9] prepared self-assembled structures (core-shell Ag nanowires and flower-like Ag NPs) and used them as SERS active substrate in order to detect melamine in ppm ranges. In this study the SERS detection was assessed by using the laser emitting at 633 nm which is actually the preferred and more appropriate laser line for this investigation [10-11], providing **limits of detection (LOD)** up to sub-ppm level. However, very promising results were obtained with other excitation laser lines too: 785 nm (LOD of 1-10 ppm) [26], 514.5 nm (LOD of 1 ppm) [27].

The ultrasensitive and straightforward method of SERS detection of these compounds at trace level coupled with the computational chemistry approach makes the here presented studies original and relevant for future investigations of similar (bio) molecules.

Several of the reported SERS applications were chosen because they have been the subject of multiple investigations, for instance the **colloidal suspensions**, and thus, they are particularly useful for comparing the relative merits of different approaches. In addition to these means of investigations, by using colloids, we also coupled **thin layer chromatography (TLC)** and SERS as a tool for the separation and identification of certain dyes, as test molecules for this innovative setup. In addition, a green, new synthesis of gold NPs by using biocompatible polymers as reducing agents is reported for the first time (the study makes the object of a **patent request at OSIM A00483/29.06.2012**, as part of the Project IDF20120002, intellectual property of **NextPhase S.A. Romania**).

By using the high sensitivity of SERS, the detection of microorganisms, particularly common UTI pathogens, was proved even at single-cell level [33-36]. Prominent medical and financial implications associated with UTIs occurred in recent years. There are still concerns related to UTIs as the risk of low-weight birth, premature delivery and fetal mortality among pregnant women or associated renal diseases in pediatrics [37]. Particularly, adult women show prevalence to UTIs; almost 50% of women will experience at least one episode of UTIs during their lifetimes [38].

Currently, UTIs can be diagnosed by using the urine dipsticks that can detect the presence of leukocytes esterase, a marker for white blood cells, therefore an indicator of an infection. Since it fails to detect the Gram-positive bacteria, this test has about 68%-88% sensitivity [39]. The false negative results occur usually in about 16% of the cases. The alternative available tests rely on nucleic acid-based **polymerase chain reaction (PCR)**, **enzyme-linked immunosorbent assay (ELISA)** [40] and **matrix-assisted laser desorption/ionization (MALDI)** [41-42], which all require an actual culture of the pathogens to test on. The cultivation step is costly and time-consuming, but unfortunately, the only cheap and fast test, the urine dipstick, needs almost always a confirmation. PCR and capture antibody-based sandwich immunoassay [43] have several potential problems, such as high rate of false negatives and false positives. Different recent approaches that possess a high sensitivity are molecular techniques, such as **fluorescence in situ hybridization (FISH)** [44] or **loop-mediated isothermal amplification (LAMP)** [45] are typically used to identify UTI causative pathogens. In these cases, the sample preparation and post-processing fluorescence imaging make them difficult and rely on highly skilled personnel.

In the case of microorganisms' detection by using SERS, the most common procedure of sample preparation is the sedimentation of the biomass on the glass slide (or a low fluorescence microscope slide) or the simple mixture of the biomass with the colloidal suspension and immediate acquisition of the spectral information [46-48]. As an alternative to the drying prior to usage procedure or the capturing of the biomass by using antibodies [35, 40,

43, 49], we propose a more straightforward and innovative receptor-free approach to immobilize bacteria by electrostatic forces.

The growing need to ensure appropriate and fast diagnosis and by further investigation to estimate the risk of developing an antimicrobial resistance is in some cases vital. Vibrational spectroscopy is a powerful tool considering the high and well-defined spectral information and the simple, mobile and cheap equipment required. SERS, by its nature of enhancing the Raman cross-sections, provides intense spectra, and in determined conditions (by generating the so-called "hot-spots") allows the detection down to the single (bio) molecule level.

Conclusively, it can be inferred that there is a great potential for applying SERS as a routine analytical technique in rapid detection of chemical or biological contaminants in foods and not only. SERS is the most appropriate investigation tool in biomedical applications due to its ultra sensitivity, its minimum sample preparation required, and its obliviousness to water, so intrinsic to biological samples. SERS requires cheap equipment and provides cost-efficient on-site investigation possibilities with limits of detection down to single-molecule level.

A major concern and thereby an investigation field that connects the proposed ultrasensitive detection methodology and the selected applications presented in this thesis is the fate of both the molecular compounds and microorganisms in the environment (industrial waste, domestic route, accumulation in animal habitats, partial degradation, etc.). This process is still under ongoing and close examination and we are confident that SERS approach can provide fast and reliable solutions to all the mentioned recent needs in pharmacy, medicine and health care systems, but also in water or environmental research.

In the case of microorganisms' detection by SERS, the most common sample preparation is drying the biomass on the glass slide and/or simply mixing the biomass with the SERS-active NPs and immediately acquiring the spectra [46-48]. As an alternative to the drying prior to usage procedure or the capturing of the biomass by using antibodies [35, 40, 43, 49], there are studies based on an innovative label-free approach to immobilize bacteria by micro contact printing onto glass or gold-plated patterned chips of siderophores [50-51], or siderophore-binding protein capturing for developing antibiotics that interfere with the bacterial iron transport [52]. Recently, a methodology of biosynthesizing Enterobactin, the primary siderophore of Gram-negative species has been developed [53]. A new approach applied for more reproducible colloidal SERS measurements was proposed by Kahraman et al. [54]. The authors reported that the most reproducible and stable SERS active substrate was obtained by using the 4 times concentrated NPs, at a pH value of at least 7, because this way the close contact of the aggregated NPs to the bacterial cell wall is guaranteed. This is mainly due to the fact that the increased concentration of NPs provides an increased probability of producing "hot-spots" and this is then reflected in the SERS spectra by enhanced specificity since more spectral information is available.

The preparation of green, simple, fast and stable SERS-active substrates is here proposed, by photo-reduction of silver nitrate treated TLC plates and also by using biocompatible (not thiolated) polymers. This way, the absence of unwanted byproducts and high biocompatibility of the developed SERS substrates provide great opportunities of their usage in biomedical applications.

Theoretical and vibrational analysis of nitrogen-rich biomedical compounds

Nitrogen-rich compounds such as **melamine** are used to fraud the tested content of protein of food stuff. The current global perspective on the chemical safety of imported foods describes monitoring of food ingredients for chemical contamination and considers toxicological and risk assessment when dealing with chemical contaminants in foods. From analytical point of view, the conventional techniques used for screening of melamine and analogues in food and feed are ELISA and HPLC-UV/diode array detector-DAD (with low selectivity and sensitivity, but also low analysis costs), gas chromatography (GC)-MS (with medium characteristics and high costs), and GC-MS/MS and LC-MS/MS (high selectivity and sensitivity but very high costs of analysis) [55-58]. Alternative methods used as promising tools for melamine analysis include spectrophotometric absorption [59], UV-vis spectroscopy [60], electrokinetic capillary chromatography [61], TLC [62] and Raman spectroscopy [32].

We investigated the feasibility of using surface-enhanced Raman spectroscopy (SERS) to detect food contaminants such as melamine in foods and food ingredients more quickly and accurately than other traditional methods. The aim of this study is to add to the analytical reports concerning melamine SERS detection, a physico-chemical characterization of both, neutral and protonated melamine molecular species, by using spectroscopic methods combined with theoretical calculations.

Melamine

Melamine, the common name for **1,3,5-triazine-2,4,6-triamine**, is a nitrogen-rich (67% per mass unit) organic compound, being a synthetic chemical used in a variety of industrial and commercial applications including the production of resins and foams, laminates, glues, cleaning products, flame retardants and fertilizers. It became well-known mostly in the last decade together with its hydrolysis products (ammeline, ammelide, cyanuric acid) [24] because it was fraudulently added to food to increase the apparent protein content which is measured by analysis of nitrogen. Intake of melamine can cause different conditions that affect the urinary tract and other health problems [63]. Melamine use in the adulteration of specific foods is allowed in many countries but the tolerable considered daily intake is **0.2 mg/kg** body

weight [55]. For these reasons, reliable and prompt detection and qualification of melamine residues and other potentially toxic contaminants in food immediately became a very important safety issue, the proficiency of several laboratories to determine melamine in food being recently assessed [5].

The pKa value of melamine in water was evaluated by Jang et al. [24] using DFT methods in combination with the Poisson-Boltzmann continuum solvation model, the obtained value, pKa 5, being in good agreement with our calculated value of 4.87 obtained by using ACD/pKa DB (ACDLABS 12.0, Advanced Chemistry Development, Inc., Canada). According to our calculations, the simple protonated species is mostly present in acid solutions, at 5-5.2 pH values and the neutral species in alkaline solutions, for pH values higher than 8.

Neutral form of melamine

The neutral molecular form of melamine was investigated by FTIR, FT-Raman and SERS spectroscopic methods, as well as by quantum chemistry. According to the DFT calculations, a planar structure is predicted for the protonated species, while a non-planar structure is the most stable in the case of the neutral form of melamine. The non-planar structure revealed by our optimization parameters and frequency calculations at B3LYP/6311++G(d,p) level of theory can be described as having two pairs of NH_2 groups pointing out to one side of the triazine ring, the other one pointing towards the opposite direction.
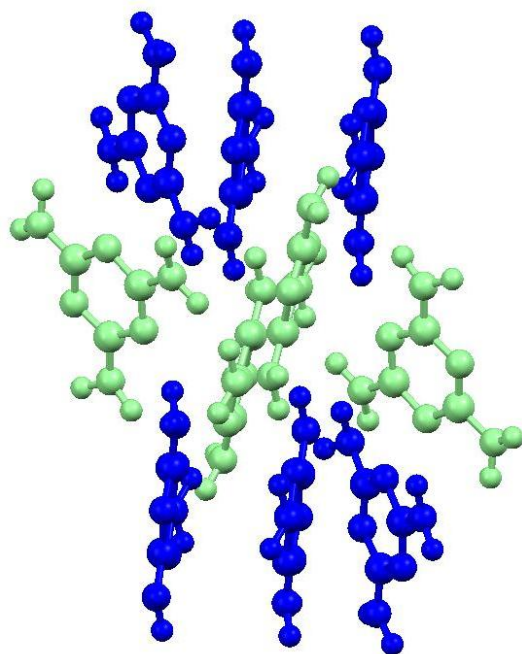

Fig. 1. B3LYP/6-31G(d) partially optimized structure of a cluster of ten melamine molecules.

Vibrational mode assignments of the calculated spectra were made by visual inspection of modes animated with the Gaussview 4.1 program [64] based on the direct comparison between the experimental and calculated spectra by considering both, the frequency sequence and intensity pattern, establishing thus a one to one correlation between the observed and theoretical calculated frequencies. For an accurate reproduction of the vibrational spectra of melamine in polycrystalline form, a cluster formed by ten melamine molecules (shown in Figure 1) was designed, starting from the X-ray structure arrangement reported by Varghese et al. [65]. Four molecules representing the unit cell extracted from the neutron diffraction crystal structure (which were free to vibrate, represented in light green) and six molecules that "pack" the unit cell (which remained frozen during the calculation, represented in blue) making hydrogen bonding possible, constituted our model. For the cluster calculation we used

the same B3LYP hybrid functional, but the less flexible 6-31G(d) basis set. The neutral molecular form of melamine was investigated experimentally by FTIR, FT-Raman and SERS spectroscopic methods. Figure 2 shows the experimental mid-infrared spectrum of polycrystalline melamine, as well as the calculated IR spectra corresponding to the single melamine molecule and to the previously described cluster.

Because melamine is low water soluble (3.24 mg/ml), the achieved concentration in water was not high enough in order to record the conventional Raman spectrum of melamine in aqueous solution. To overcome this inconvenience, the FT-Raman on powder was recorded and SERS spectroscopy was employed, the SERS spectrum of melamine neutral molecular form being recorded in silver colloidal solution at pH 8. Figure 3 shows the FT-Raman spectrum of melamine powder, the SERS spectrum and the DFT calculated Raman spectra of the melamine ten molecules cluster.
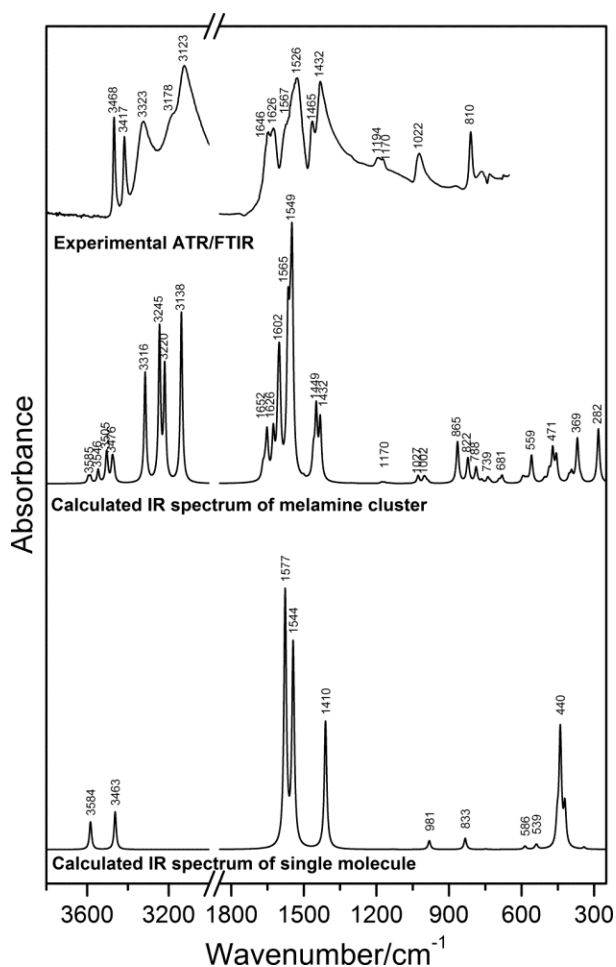

Fig. 2. ATR/FTIR spectrum of melamine powder (top), the calculated IR spectrum of a cluster of ten melamine molecules (middle) and the calculated IR spectrum of a single molecule in neutral form (bottom).
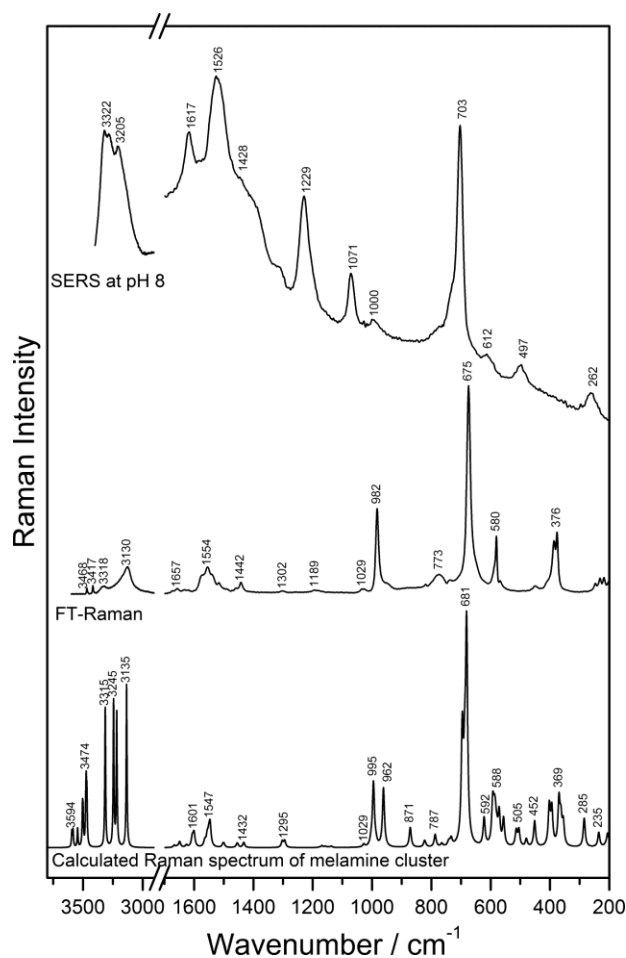
Fig. 3. Calculated Raman spectrum of ten melamine molecules cluster (bottom), FT-Raman spectrum of melamine powder (middle) and SERS spectrum at pH 8 of neutral species of melamine (top).

The experimental FT-Raman spectrum is reproduced satisfactorily by the DFT calculated spectrum of the ten melamine molecules cluster and is dominated by marker bands as the ring breathing vibration, observed as an intense band at 675 cm^{-1}, whereas in the calculated spectrum this band is present at 681 cm^{-1}. This total symmetric stretching vibration of the ring is shifted to 703 cm^{-1} in the SERS spectrum, due to the interaction of melamine with the silver surface. Another Raman marker band of melamine is the band at 982 cm^{-1} in the FT-Raman spectrum, present in the calculated spectrum at 995 cm^{-1}, assigned to CNC+NCN bending vibration. In the SERS spectrum this band is shown at 1000 cm^{-1}. The most enhanced bands in the SERS spectrum appear at 703 cm^{-1},1071 cm^{-1} and 1229 cm^{-1}, assigned to ring stretching, ring in plane deformation as well as NH_2 groups deformation vibrations. A more detailed assignment of the experimental Raman and DFT calculated bands of neutral melamine is shown in Table 1. In bold are mentioned the percentage contributions for the neutral melamine and in italics the contributions for the protonated one. The last column contains the motions that contribute the most to different normal modes according to B3LYP/6-311++G(d,p) level of theory.

Protonated form of melamine

Theoretically and also from literature [23-24], it is known that protonation of melamine occurs at the endocyclic N-atoms in the triazine ring. Based on UV-absorption experiments, Hirt and Schmitt [66] also predicted that the endocyclic N-atoms are more basic than the NH_2 groups. The single protonated form of melamine can occur by protonation on either one of the nitrogens of the triazine ring, the three protonation sites being, however, equivalent. Conclusively, the ring protonated form was considered in order to establish a correlation between the pKa values and the electronic-energy levels and atomic charges.

Conversely to the neutral form, as a result of the B3LYP/6-311++G(d,p) level of theory optimization calculations, in the case of the protonated species, we found a completely planar structure, even if we used as a starting geometry a structure significantly distorted from planarity.

Because of its low solubility in water, conventional Raman spectra of protonated melamine in aqueous solution could not be recorded with the used setup. However low melamine concentration in silver colloid at pH 4 was used to record the SERS spectrum. Figure 4 presents the obtained SERS spectrum and the spectrum of the protonated form of single melamine molecule, calculated at B3LYP/6311++G(d,p) level of theory.

SERS spectra of melamine at different pH values (pH 3, 7, 12) were recorded using silver colloids and the sensitivity (at detection limit) of the SERS method was evaluated. By comparing the SERS spectrum of the protonated melamine molecular species with the SERS spectrum of neutral melamine (Figure 5) several marker bands are revealed as characteristic to

each species. For instance, the band at 1228 cm^{-1}, specific to the neutral molecular form, is assigned to ring stretching of melamine. Another specific vibration, but for the protonated species, is the triazine trigonal bending (δ(CNC)+δ(NCN)) present at 979 cm^{-1} in the SERS spectrum and at 981 cm^{-1} in the calculated spectrum.

Present in both protonated and neutral molecular species SERS spectra are marker bands as: the triazine ring breathing vibration, at 686 cm^{-1} and 700 cm^{-1}, respectively; the triazine trigonal bending (δ(CNC)+δ(NCN)) vibration at 978 cm^{-1} and 985 cm^{-1}, respectively. These results are in very good agreement with those reported by Pekparlak et al. [67], including the experimental IR and Raman spectra section, which fully support the assignments of the most important bands discussed for our SERS spectra.
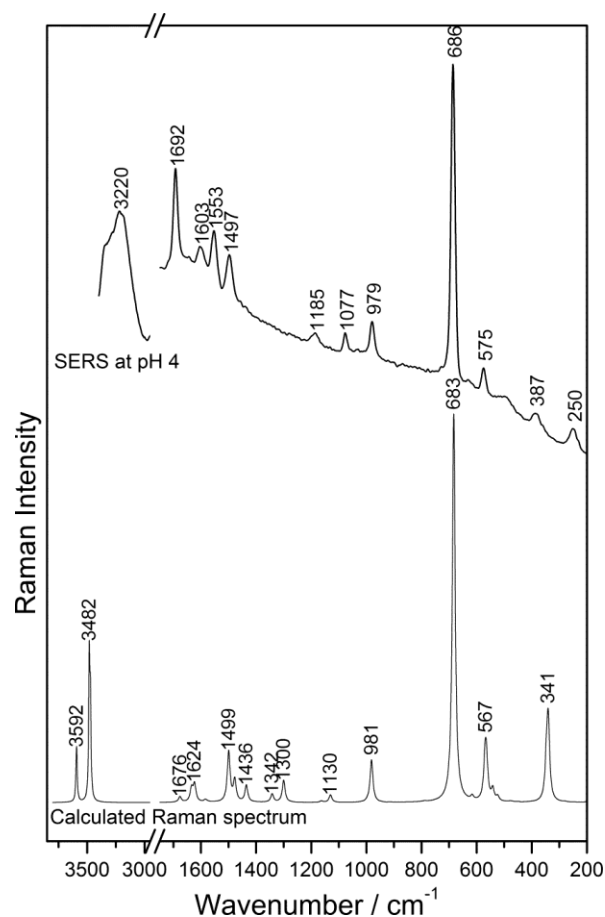

Fig. 4. SERS spectrum (top) at pH 4 and calculated Raman spectrum (bottom) of the protonated molecular form of melamine.
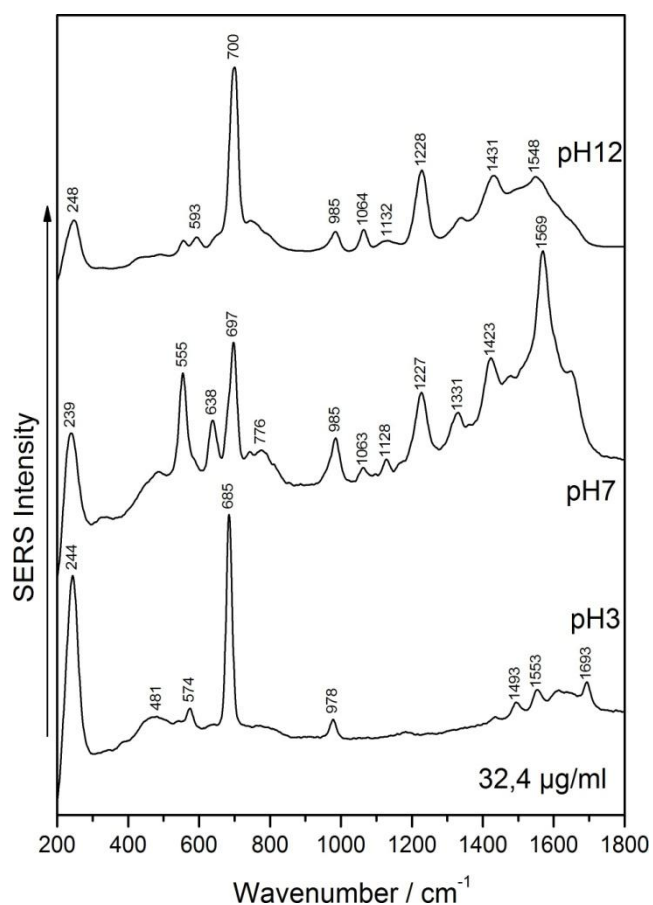

Fig. 5. SERS spectra (from top to bottom) of melamine at pH 12 (neutral molecular form), pH 7, pH 3 (protonated molecular form) recorded at a concentration of melamine of 32.4 µg/ml.

Table 1. Experimental ATR/FTIR, FT-Raman and SERS, as well as calculated wavenumbers (cm^{-1}) of IR and Raman active vibrational modes of neutral and protonated molecular species of melamine

Experimental				Calculated IR		Calculated Raman		Assignment	Calculated contribution (%) of the normal mode
IR neutral	Raman neutral	SERS neutral	SERS protonated	Single molecule neutral	Cluster neutral	Cluster neutral	*Single molecule protonated*		
	376		387			369	341	δ(CN)	*65.2*
	580	612	575	569		588 592	569	δ(NCN) + δ(NH$_2$)	**26.8**(*40.5*)
	675	703	686			681	683	ring breathing	*28.3*
810				833	822			ring out-of-plane def	**49.2**
	982	1000	979	981		962 995	981	δ(CNC)+δ(NCN)	**9.5+9.9**(*9.5+38.5*)
1022	1029	1071	1077		1027	1029		ring def+ρ(NH$_2$)	*17.8*
1170 1194	1189				1170	1170		ring def+ρ(NH$_2$)	*25.1*
	1302	1229				1295	1300	δ(NH)	*29.2*
1432 1465	1442	1428		1410	1432 1449		1436	ν(CN)+δ(NH$_2$)	**36.6+12.4**(*34.2+33.9*)
		1526	1497				1499	δ(NCN)+ω(NH$_2$)	*13.9+27.6*
1526 1567				1544	1549 1565			ν(CN)+δ(NH$_2$)	**31+30.1**
	1554		1553	1577		1547		δ (NH$_2$)	**53**

1626 1646		1617	1603		1602 1626 1652	1601	1624	δ (NH$_2$)	*41*
	1657		1692			1649	1676	δ (NH$_2$)	*44*
3123 3178 3323 3417 3468	3130 3318 3417 3468	3205 3322	3220	3465 3584	3138 3220 3245 3316 3476 3505 3546 3585	3135 3218 3245 3315 3474 3503 3546 3585 3594	3482 3592	ν(NH)	***87.9****(85.8)*

Legend: def. – deformation, ω-wagging vibration, δ-bending vibration, ν-stretching vibration, τ-twisting vibration

Melamine adsorption to the silver surface

The adsorption of melamine to the silver surface was inferred based on the MEP contour map and SERS marker bands. As can be observed in Figure 6, the highest electron density is located on the ring nitrogens, thus the molecule is supposed to adsorb through these atoms. The spectral features confirm the chemisorption of melamine molecule to the silver surface by the Raman shift of the 675 cm^{-1} and 1554 cm^{-1} bands, due to the interaction of melamine with the silver surface towards 703 cm^{-1} and 1526 cm^{-1} respectively.
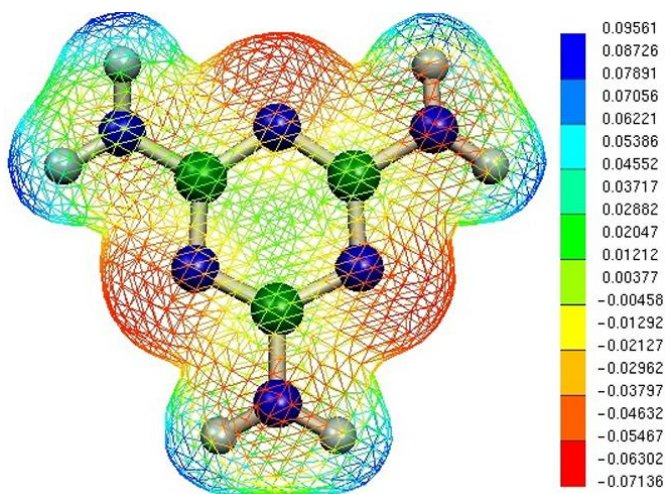

Fig. 6. B3LYP/6-311++G(d) calculated 3D electrostatic potential of neutral melamine (a.u.) mapped onto the electronic isosurface of 0.02 a.u.

To predict reactive sites for melamine, the B3LYP/6-311++G(d) calculated 3D MEP contour of neutral melamine was mapped onto the electronic isosurface of 0.02 a.u. The orientation with respect to the metal surface of the adsorbed melamine molecule can be inferred based on the SERS surface selection rules [68-70]. Accordingly, the normal modes with a change in polarizability component perpendicular to the surface are enhanced. For both molecular species, neutral and protonated, the most intense SERS band is due to the ring breathing vibration, therefore, a predominant perpendicular ring orientation of melamine with respect to the silver surface is supposed.

In conclusion, a physico-chemical characterization of neutral and protonated melamine molecular forms was performed, including the recording of the FTIR, FT-Raman and SERS spectra with a fair band assignment based on DFT calculations. The experimental FTIR and FT-Raman spectra of melamine are satisfactorily reproduced by DFT calculations if intermolecular hydrogen bondings are also considered, as shown by the calculated IR and Raman spectra of the melamine ten molecules cluster. The SERS spectra of neutral and protonated melamine molecular species show distinct spectral features, as revealed by specific marker bands. SERS represents a reliable complementary method for conventional chromatographic and immuno-based assays that could provide a fast and ultrasensitive tool for melamine monitoring. The limit of detection in SERS detection of melamine in aqueous solutions was 32.4 μg/ml, low enough to be used in food safety assays.

Zidovudine

Zidovudine, 3'-azido-3'-deoxythymidine (AZT) is a molecule of pharmacologically relevant, being member of the class called nucleoside-analog reverse transcriptase inhibitors, used to delay development of AIDS in patients infected with HIV. HIV is capable of mutating so it can become AZT-resistant over time, and for this reason AZT is usually used in conjunction with other nucleoside reverse transcriptase inhibitors (NRTIs) and anti-viral drugs. Zidovudine is also used as a new radiosensitizer in cancer radiotherapy, being able to suppress telomerase activity (TA), decrease the repair rate of the DNA strand breaks (terminate duplication of virus RNA) and increase radiosensitivity in human malignant glioma cell line U251 [15]. In newborn treatment, zidovudine added to nevirapine reduced mother-to-child transmission of HIV approximately 36% [71]. In order to avoid toxicity and also to achieve optimal drug concentration for viral suppression, it is now recommended a careful monitoring of drug levels [4].

In order to optimize the experimental conditions for SERS spectroscopy, a physico-chemical study is necessary to identify which molecular state (protonated, neutral, deprotonated) is favored for the adsorption to metal nanostructures, thus generating a higher SERS intensity. The physical processes and chemical reaction involved in biological processes are often very sensitive to the concentration of the hydrogen ions of the medium. The concentration of a drug in tissue for example, at a given time, depends on the absorption, distribution and elimination of that drug. The kinetics of these processes is dependent on the pK_a values of the drug [72]. For this purpose, the pK_a values of AZT depending on the pH domain were calculated using ACDLABS 12.0 (Advanced Chemistry Development, Canada) software. The pK_a value 9.55 was determined, the pK_a value of 9.78 being predicted in a previous study by Checa et al. [73]. At this pH value, both species identified, namely the neutral molecular form of AZT (predominantly present in the 5-9 pH range), and the simple deprotonated species (present at alkaline pH=12) are present with equal contributions.

The vibrational study was coupled with DFT calculations at B3LYP/6-31G(d) level in order to accurately assign the vibrational normal modes. The study of conformation and adsorption mechanism of AZT in solution at different pH values and when adsorbed on metal surfaces is also of paramount importance. For instance, MEP can describe the recognition process between the ligand and the drug-actives sites, along with other significant processes for the biological activity anti-HIV [21].

The so far reported spectroscopic studies of AZT and its derivatives include IR and Raman spectra, usually in comparison to other small azide compounds of AZT's thymine moiety [1, 17, 25]. The single SERS study reported by Rivas et al. [16] includes the investigation of the adsorption mechanism on the silver surface in accordance with the SERS selection rules. The theoretical reported studies on AZT by using DFT calculations are focused on the conformational behavior and the MEP of the molecule [21, 25, 74]. The molecular geometry

optimization and vibrational wavenumbers calculations included in our theoretical study were performed with the Gaussian 03W software package [75] at B3LYP/6-31G(d) level of theory, both in the case of the neutral and simply deprotonated forms. Figure 7 shows the B3LYP/6-31G(d) optimized molecular structure of neutral zidovudine in gas-phase with atom numbering for a facile visualization and assignment of the vibrational modes.
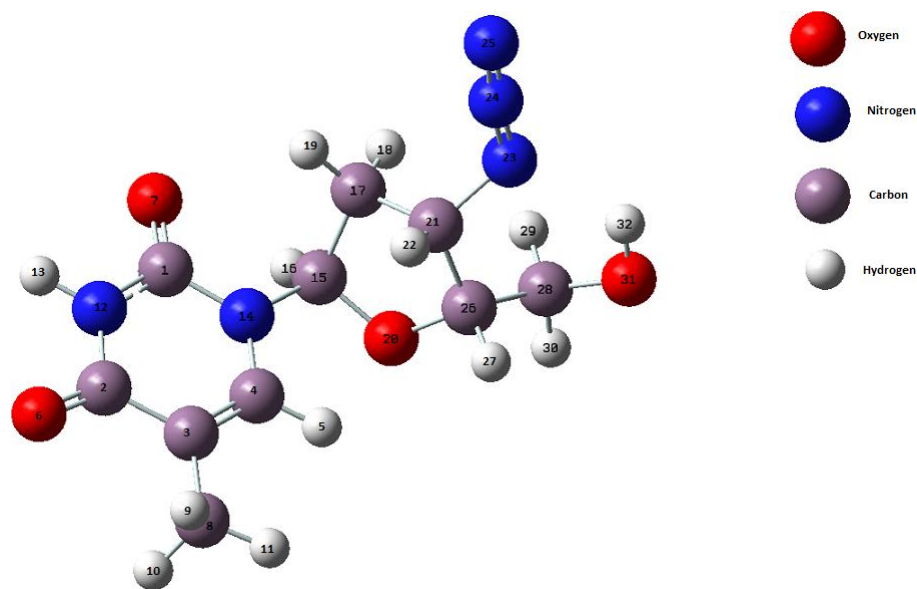

Fig. 7. B3LYP/6-31G(d) optimized molecular structure of neutral zidovudine in gas-phase.

The main IR active vibrations of AZT are the OH stretching mode at 3460 cm^{-1} and the C=O stretching mode at 1676 cm^{-1} (see Figure 8 inserted below, showing the FTIR spectrum and the B3LYP/6-31G(d) IR calculated spectrum) as also reported by Kruszewska group [1]. Owing to the high polarity of the azido (N=N and N≡N bonds) group, the additional intense vibrations in IR spectrum are the two stretching vibrations of azido group, between 2080-2130 cm^{-1} (for N≡N bond) and 1210-1290 cm^{-1} (for N=N bond). This assumption is also supported by MP2(full)/TZ2P (post Hartree Fock level of theory) calculations which assign these spectral features to the azido group as detailed above, rather than to the two (NNN) asymmetric and symmetric stretching modes [25].

Figure 8 shows the FTIR spectrum and the B3LYP/6-31G(d) IR calculated spectrum of neutral zidovudine and by comparing these spectra, shifting is observed in IR active bands. Furthermore, by using the optimized geometries to calculate the vibrational frequencies in water solvent based on the Polarizable Continuum Model (PCM) solvation model, we obtained the calculated wavenumbers for the aqueous solution of neutral zidovudine as well. The wavenumbers and their assignments are included in Table 2.

Table 2. IR experimental and B3LYP/6-31G(d)calculated wavenumbers of zidovudine and their assignments.

FTIR experimental Wavenumbers (cm^{-1})	IR gas phase calculated Wavenumbers (cm^{-1})	IR solvent model calculated Wavenumbers (cm^{-1})	Assignments
760	766	761	$\rho(C_8H_3) + \delta(N_{12}>C_2>H_{13})$
790		776	$\omega(N_{12}H_{13})$ + rings breathing
934	933	943	$\omega(C_4 H_5)$
1088	1084	1076	$\rho(CH)$
1143	1141	1142	$\omega(C_{15}H_{16}) + \rho(CH)$
1259	1257	1256	$\omega(CH_2)$
1279	1285	1290	$\omega(CH) + \nu_s(N=N)$
1380	1377	1378	$\omega(C_{15}H_{16})$
1403	1395	1394	$\omega(C_8H_3)$
1466	1464	1471	$\rho(C_8H_3)$
1676	1724	1674	$\nu_s(O_6=C_2) + \delta(N_{12}H_{13})$
2984	2996	2982	$\nu_s(CH_2)$
3460	3461	3454	$\nu_s(N_{12}H_{13})$

FT-Raman recorded spectrum and the B3LYP/6-31G(d) Raman calculated spectrum of neutral zidovudine are shown in Figure 9. As easily can be observed, the Raman bands specific to the azide group are dominant. This fact was also underlined by the conformational study that refers to the FT-Raman and SERS spectra of AZT in the 2.5-10.5 pH range of Rivas et al. [16] that points out also as the main spectral features the Raman bands at 1688 cm^{-1}, assigned to the C=O stretching mode, at 2117 cm^{-1}, ascribed to the azide group. The study reported by Raviolo et al. [19] exhibits the Raman spectrum of AZT carbonate recorded with another laser line, 514.5 nm, and refers to the C=O stretching mode at 1715 cm^{-1}, to the asymmetric (O-C-O) stretching vibration at 1240-1280 cm^{-1} and in-plane bending skeletal mode of (NH/CH) or (CH$_3$/CH) between 1430-1475 cm^{-1}. In this case the titration took place for DMSO solutions of an AZT carbonate, a novel compound synthesized by the above mentioned research group. The FT-Raman spectrum also exhibits at 1235, 770, 496 cm^{-1} the thymine bands; at 867, 847, 736 cm^{-1} the deoxyribose bands and at 1356 and 1390 cm^{-1} thymine in-plane bending CH vibration are observed.
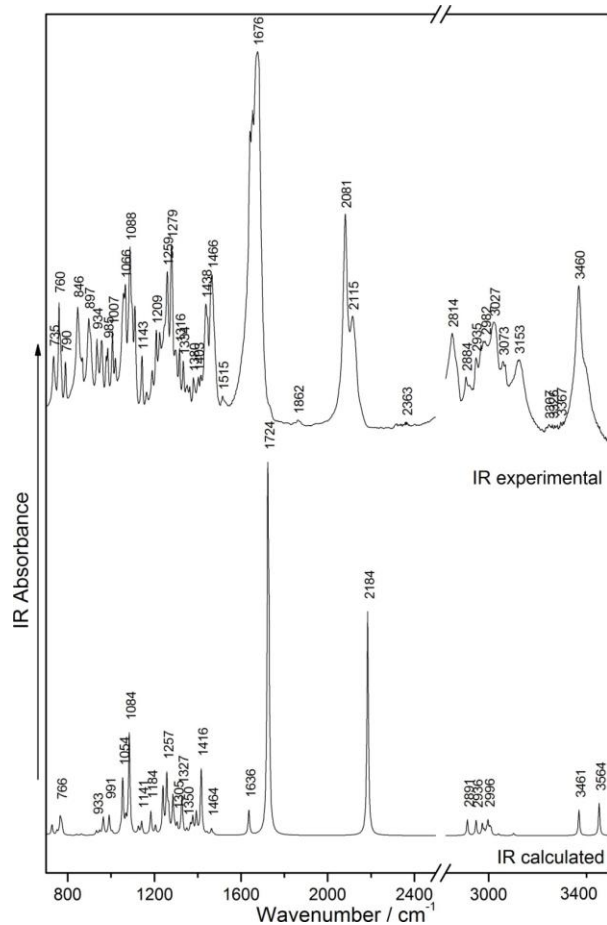
Fig. 8. FTIR spectrum of zidovudine and B3LYP/6-31G(d) IR calculated spectrum of neutral zidovudine.
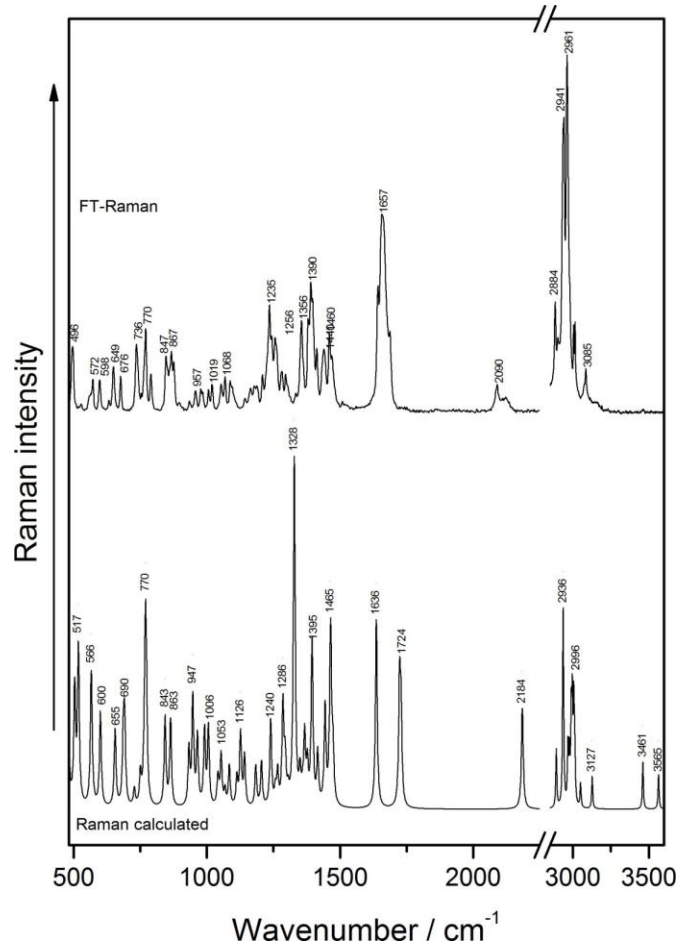

Fig. 9. FT-Raman and B3LYP/6-31G(d) Raman calculated spectra of neutral zidovudine.

Aqueous solutions of zidovudine were prepared, in distilled water, in order to detect different concentrations of zidovudine by SERS. Figure 10 shows SERS spectra of aqueous solutions of 10^{-4} M zidovudine at pH 7 and pH 12. The enhanced bands are slightly shifted from one recorded spectrum to another. However, there are some bands that suffer shifting in comparison with the FT-Raman spectrum as well: the 1657 cm^{-1} band shifts to 1644-1649 cm^{-1} (vibration ascribed to the C=O stretching mode), 770 cm^{-1} ring breathing mode band shifts to 791 cm^{-1}, 1235 cm^{-1} shifts to 1243-1252 cm^{-1}. All these bands are proof of the interaction of AZT with the silver surface through the thymine residue. The tentative assignments of the Raman and SERS spectra are displayed in Table 3.

In the SERS spectrum recorded in aqueous solution, at neutral pH, the 1657 cm^{-1} Raman band (Raman spectrum recorded on powder) shifts to 1649 cm^{-1} (C=O stretching) as interaction of AZT with the surface through the thymine residue.
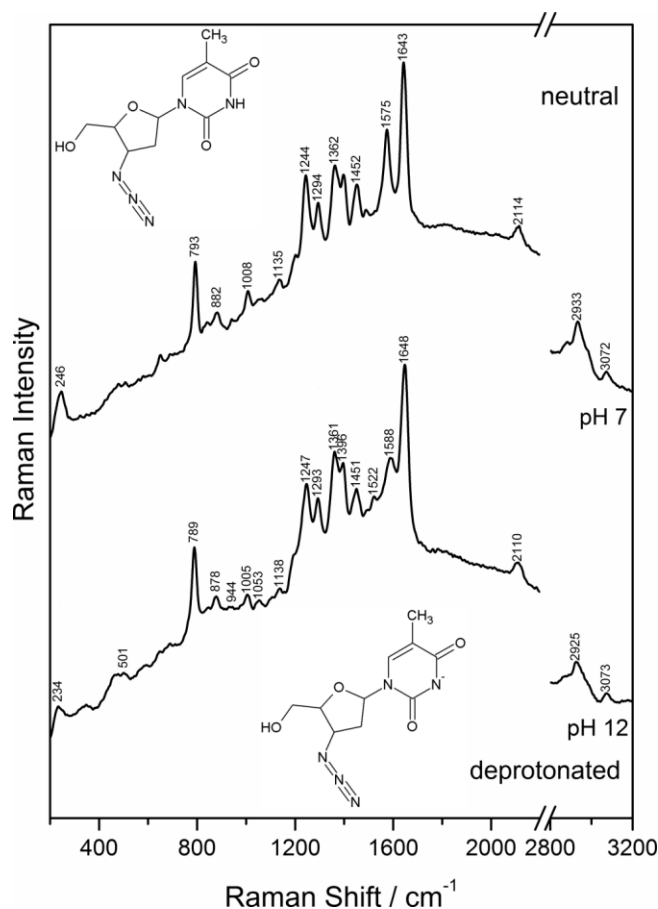
20

Fig. 10. SERS spectra of 10^{-4} M zidovudine at pH 7 and pH 12 (normalized and baseline corrected).

Preparing different pH environments, we monitored the two species of zidovudine, the neutral one in the 3-7 pH values interval, and the deprotonated one, at pH=12 (see the structure in Figure III.15.). Comparing the two corresponding SERS spectra (included in Figure III.14.), it is evident that Raman shifting is notable mostly for the band at 1588 cm^{-1} in the case of the deprotonated zidovudine, assigned to the symmetric stretching vibration of the (C=C) and (C=O) bonds in the six-membered ring (ring 2), which is shifted for the neutral species to 1575 cm^{-1}, simultaneously with an enhanced intensity. The SERS band at 793 cm^{-1} for the neutral form is shifted at 789 cm^{-1} in the spectrum of the deprotonated species, being assigned to the symmetric stretching vibration of the (C-C) bonds in the ribose ring. The most intense band in the vibrational spectrum of the neutral species is that observed at 1643 cm^{-1}, which is shifted at 1648 cm^{-1} for the deprotonated molecular form, maintaining its intensity.

Table 3. Selected experimental and calculated Raman shifts for zidovudine

Experimental wavenumbers (cm^{-1})			Calculated wavenumbers (cm^{-1}) [B3LYP/6-31G(d)]		Assignments
Raman	SERS (n)	SERS (d)	Raman (n)	Raman (water)	
496	-	-	517	480	$\omega(O_{31}H_{32})$
770	793	789	770	767	Deformation of ring 2
867	882	878	863	865	$\delta(C-H)$
1235	1244	1247	1240	1240	$\delta(C-H)$ in both rings
-	1294	1293	1286	1290	$\delta(C-H)+v (N=N=N)$
1356	1362	1361	1359	1362	$\delta(N_{12}H_{13})+\delta (C_4H_5)$
1390	-	-	1395	1394	$\delta(C-H)$
-	1575	1588	-		$v_s(C=C)+v_s (C=O)$ [ring 2]
1657	1643	1648	1636	1629	$v_s(C3=C4)$
-	-	-	1724	1700	$\delta(NH)+v_s (C=O)$ [ring 2]
2090	2114	2110	2184	2172	$v(N=N=N)$
2941	2933	2925	2936	2933	$v_s(C_8H_3)$
3085	3072	3073		3050	$v_{as}(C_{17}H_2)$

Legend: ω-wagging vibration, δ-bending vibration, v-stretching vibration; n-neutral form, d-deprotonated form of zidovudine

The adsorption of zidovudine to the silver surface was inferred based on the molecular electrostatic potential (MEP) contour map and several marker bands. In order to study the adsorption and assembly mode of molecules one can additionally employ SERS spectroscopy, which affords additional information about the structure distorted by adsorption or about the electro-dynamical properties of (bio) molecules. MEP is widely used as a reactivity map, displaying most probable regions for the electrophilic attack of charged point-like reagents on organic molecules [76].

As it can be seen in the MEP distribution of neutral zidovudine molecule obtained from DFT calculations depicted in Figure 11, the negative charge is located mainly on the oxygen atoms, thus it is supposed that zidovudine absorbs to the silver surface by the oxygen atoms of the thymine ring. This supposition is sustained by the strong shifting of the C=O band of the thymine moiety. The site of deprotonation and the possible adsorption geometry was studied by Rivas et al. [16]. They concluded that the AZT interacts with the silver surface through the N atom (ring, NH atom), which undergoes a deprotonation similar to that occurring in silver complexes of DNA [16]. On the metal surface, the thymine ring seems to adopt an almost perpendicular orientation as suggested by the enhancement of the ring breathing mode and of the 3073 cm^{-1} band (also in accordance with the SERS selection rules). The presence of the C=O stretching vibration as well as of the breathing vibration of the thymine ring as intense bands in the SERS spectra indicates a predominant per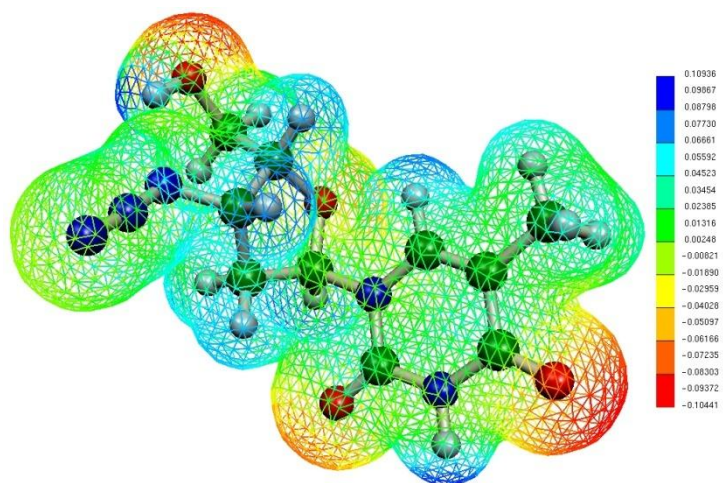pendicular orientation of the thymine ring as well, deduced from the SERS selection rules [69, 77]. A predominant parallel orientation of the ribose ring, with respect to the silver surface is proposed, due to the weak SERS bands associated with this ring. It has to be mentioned, that the N=N=N stretching vibration is present in the SERS spectrum at 2114 cm^{-1}, thus we suggest a tilted orientation of this group in respect to the silver surface.

Fig.11. B3LYP/6-31G(d) calculated 3D molecular electrostatic potential of zidovudine in a.u mapped on the electronic density isosurface of 0.02 a.u.

The SERS spectral features (Figure 10) confirm the chemisorption of the zidovudine molecule to the silver surface by the shift of the SERS marker bands (789, 1643, 3073 cm^{-1}), due to the interaction of zidovudine with the silver surface.

By employing a MEP study, we were able to deeply understand and visualize the adsorption mechanism of AZT on the silver surface. The limit of detection in SERS detection of melamine in aqueous solutions was 10^{-5}M.

The synthesis of new SERS-active substrates

In situ silver spot preparation and *on-plate* SERS detection in thin layer chromatography separation

Development of SERS sensing approaches represents a goal for many research groups. This general aim brings about a lot of interesting new concepts and ideas whose success and impact may be judged over the years by their implementation in commercial instrumentation. SERS has the potential of a molecular specific, high sensitive detection method. Thus, it could be more advantageous compared to conventional UV-Vis absorbance or fluorescence used routinely for detection in chromatographic separation methods, like LC and TLC, as well as in capillary electrophoresis (CE). The most common nanostructures used to enhance Raman signal are fabricated as isolated NPs (spheres [78], nanorods [79]), nanowires [80], nanoarrays [81-82] or as thin films [83-84]. Usually, in many applications of SERS the nanostructures are patterned on a solid substrate in order to obtain the necessary "roughness" of the substrate. The present study proposes the development of a simpler system, by coupling a separation method, TLC with a detection **method that provides molecular specific information**, ultrasensitive Raman spectroscopy (SERS). The TLC-SERS approach will be capable to provide **rapid analysis, high sensitivity** and also a **significantly lower analysis price**. Furthermore, such a detection system can be miniaturized and used as a mobile sensor.

Thin layer chromatography (TLC) is used to separate physical mixtures. TLC is performed on a glass plate, plastic or aluminum foil that is coated with a thin layer of adsorbent material (**stationary phase**), usually silica, aluminum oxide, or cellulose. After the sample is applied on the plate, the end of the stationary phase is then immersed in a quantity of solvent, which serves as the **mobile phase**. The solvent migrates along the stationary phase, separating the components due to polar interactions between stationary phase and sample molecules. Spot visualization is performed usually with UV light. If necessary, a fluorescent substance is applied on the plate.

As in the case of other analytes of medical or technological interest, the analysis of dyes was also significantly improved thanks to the introduction of both of chromatographic and spectroscopic techniques. Conventional techniques embrace, in the first place, UV-vis absorbance spectroscopy, which has allowed positive identification of several Anglo-Scandinavian textiles [85]. UV-vis reflectance spectroscopy was also evaluated as an alternative, for leading to satisfactory results, without the need to take a sample [86]. In the last few years, fluorimetry has also been successfully applied to the non-destructive study of pigments and colorants from medieval illuminations, paint cross sections, millenary textiles and wall paintings [87-88]. However, if a sufficient amount of sample is available for analysis; chromatographic techniques are generally preferable, as they enable separation and reliable

identification of individual components in dye mixtures. Among them, TLC was firstly applied to the investigation of madder samples in 1968 [89] and has thenceforth found increasing application in the analysis of organic colorants.

Among the vibrational spectroscopic techniques that have been evaluated for the analysis of organic colorants, e.g. FTIR [90] and NIR [91] spectroscopies, Raman spectroscopy has the greatest potential for the analysis of minute amounts of dyes and has thus been used to characterize both natural and synthetic pigments [92-94]. However, this spectroscopic technique has proven to be more suitable for the non-invasive analysis of inorganic coloring materials, as it suffers from inherently weak signals. Moreover, strong molecular fluorescence from organic dyestuffs often precludes the measurement of Raman scattering (several organic colorants are extremely fluorescent even when using relatively high wavelengths, namely 785 nm, for excitation).

In recent years, the potential of SERS as an ultrasensitive detection of organic molecules has been widely appreciated and exploited. In fact, SERS has lately found increasing application for dye investigation in works of art and archaeological objects, thanks to its great potential in providing specific vibrational fingerprints even for extremely fluorescent colorants with high selectivity and sensitivity [95-96]. The same SERS procedure was successfully applied to the identification of commonly used dyes by coupling SERS detection with chromatographic methods [97-101]. A comprehensive review [102] describes various methods of coupling Raman spectroscopy with liquid separation techniques, including CE [103-105] or even TLC separation followed by spraying the silver colloid and then SERS detection [106]. The detection limits in these conditions were reported between 1 μM for riboflavin and nM for Rhodamine 6G [104], or between 0.2 ppm and even ppb for some analytes [107].

An improved approach for SERS detection of constituents of binary mixtures after TLC separation has been developed and is here reported [108]. A SERS active silver substrate was prepared under open air conditions, directly on the thin silica film by photo-reduction of silver nitrate, allowing the detection of binary mixtures of cresyl violet, bixine, crystal violet, and Cu(II) complex of 4-(2-pyridylazo)resorcinol – $Cu(PAR)_2$. By using the recorded SERS spectrum which provides a unique spectral fingerprint for each molecule, the identification and vibrational characterization was assessed and the use of analyte standards was avoided.

Recently, our group has reported an improved methodology for the SERS detection in CE, by using a silver spot obtained by laser photo-reduction in the detection window, time resolved SERS spectra for different analytes being shown [100]. After TLC separation, in most studies, the addition of the silver colloid on the TLC plate separation point is carried out in order to enhance the Raman signal [107], with a few exceptions (for instance, Horvath et al. used vacuum deposition of the metallic substrate [109]).

In this work, we propose a more straightforward method of coupling TLC and SERS, by a pretreatment of the TLC plates with silver nitrate. This methodology enables one to create the SERS active substrate on a separated analyte region on the TLC plate and to identify the

analytes by their specific spectral fingerprints, thus avoiding the use of standards.

First of all, an effective experimental protocol for the pretreatment of the TLC plates was optimized and the most rapid and efficient procedure was then selected and followed in each experiment. The TLC plates were freshly pretreated (by simple immersion) with silver nitrate solution (10^{-2} M) for 30 s and then dried by heat in order to be further ready-to-use. By using a microliter Hamilton syringe, an approximate amount of the 0.5 µl analyte mixture was dropped on the dried, pretreated TLC plate, by forming a thin horizontal line. The used mixtures were: Cu(PAR)$_2$ (10^{-5} M)/bixine (5×10^{-4} M), cresyl violet (10^{-5} M)/Cu(PAR)$_2$ (10^{-5} M) and crystal violet (10^{-5} M)/bixine (5×10^{-4} M). In each case, the TLC plate containing the analyte mixture was placed vertically in a 50 ml beaker containing a water: ethanol (2:3) eluent and monitored until the analytes stopped ascending on the TLC plate. In 15 min, the separation was complete thus the laser from the Raman spectrometer was focused on each separated component on the TLC plate. Figure 12 is showing the used detection setup.

After 10 seconds, due to photo-reduction of silver on the plate, a SERS active silver substrate of the dimension of the laser focus (approx. 0.7 mm in diameter) was formed (see Figure 13) and the analytes adsorbed to the silver substrate, giving rise to a strong enhancement of the Raman signal. For each SERS measurement, 4 spectra were acquired by using the 4 s integration time, with a resolution of 8 cm^{-1}.
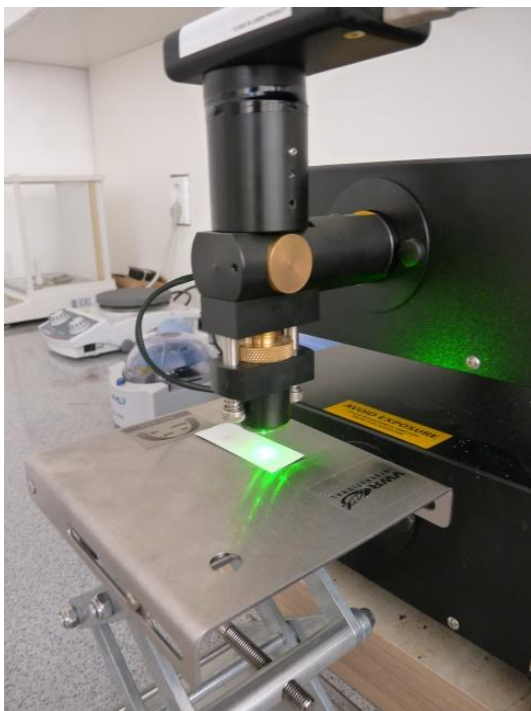
Usually, for reduction of Ag^{+} to Ag^{0}, reducing agents like citrate [110], borohydride [110], or hydroxylamine [111] are used. The main advantage in the present approach is that for the detection of pigment analytes on the TLC plate, the presence of an additional chemical reducing agent was not necessary since the silver substrate is formed by the action as reducing agents of the analyte itself, in the presence of a laser light.
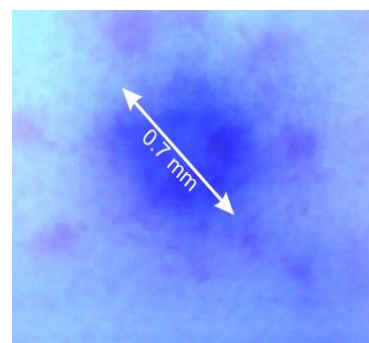

Fig.12. The detection setup used for the binary mixtures TLC separation and SERS identification.

Fig. 13. On plate SERS active silver substrate formed by photo-chemical reduction.

Figure 14 shows the SERS spectra of Cu(PAR)$_2$ and bixine recorded after a separation of their binary mixture on the AgNO$_3$ pretreated TLC plate. The resulted spectral patterns were

carefully inspected and discussed by taking into account the previously reported data [112-117]. The SERS spectrum of bixine shows the following predicted vibrational bands: the medium band at 1005 cm^{-1} which is associated with in-plane rocking CH$_3$ mode and the strong bands at 1153 and 1519 cm^{-1} associated with the stretching of the C=C and C–C bonds specific to trans-bixine [116].

Figure 15 shows the SERS spectra of cresyl violet and Cu(PAR)$_2$ complex recorded after the separation of their binary mixture on the TLC plate. The SERS specific bands of cresyl violet at 492, 523, 591, 673, 751, 830 and 946 cm^{-1} are also reported by Fujiyoshi et al. [115]. The most intense bands of dissolved cresyl violet appear at 1640 and 591 cm^{-1} and are caused by in-plane vibrational modes. The limit of detection obtained for cresyl violet was 10^{-5} M.

Figure 16 shows the SERS spectra of crystal violet and bixine recorded after the TLC separation of their binary mixture. The SERS spectrum of crystal violet exhibits the following specific vibrational bands at: 808 cm^{-1}, assigned to the out-of-plane ring C–H bending vibration, 911 cm^{-1} assigned to the ring skeletal vibration of radical orientation, 1176 cm^{-1} assigned to the in-plane C–H bending in the hydrocarbon ring, 1370 cm^{-1} assigned to the N-phenyl stretching vibration, and 1593/1623 cm^{-1} assigned to the aromatic C–C stretching vibration. The limit of detection obtained in the case of crystal violet was 10^{-5} M.

The pretreatment of TLC plates with silver nitrate solution enables, after TLC separation, the on-plate creation of a SERS active silver spot which permits the detection of analytes separated from complex matrices on the plate. The success rate was higher than 90% with a

Fig.14. SERS spectra of Cu(PAR)$_2$ and bixine recorded after a separation of their binary mixture on the AgNO$_3$ pretreated TLC plate.

detection limit below µM concentrations. This setup can now be applied to more relevant systems such as the detection of drugs, water pollutants or food additives where an online detection is highly appreciated. The development of noninvasive approaches will ultimately allow SERS to become an analytical tool of general applicability in the art conservation field.
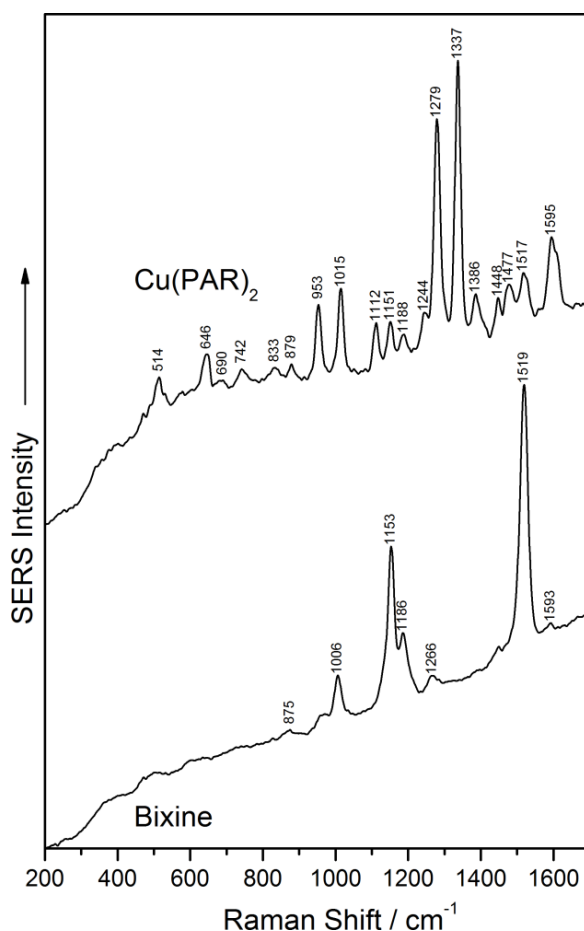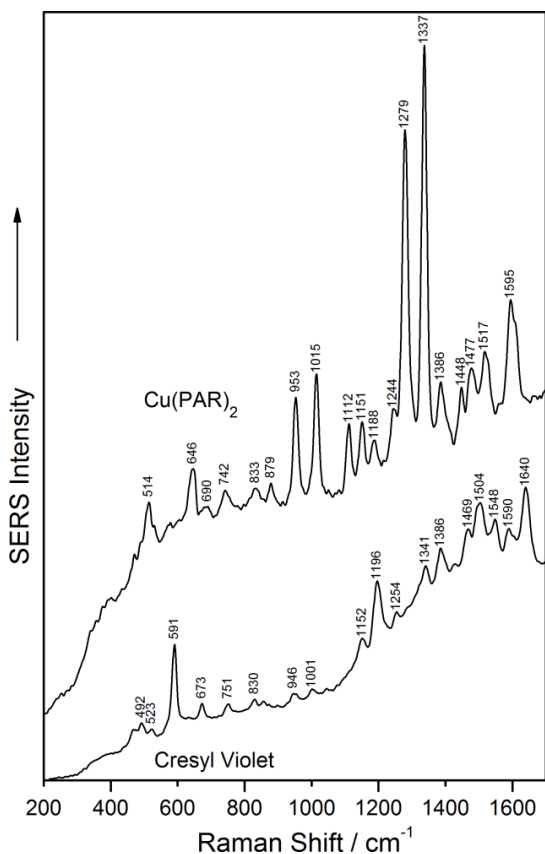
Fig.15. SERS spectra of Cu(PAR)₂ and cresyl violet recorded after a separation of their binary mixture on the AgNO₃ pretreated TLC plate.
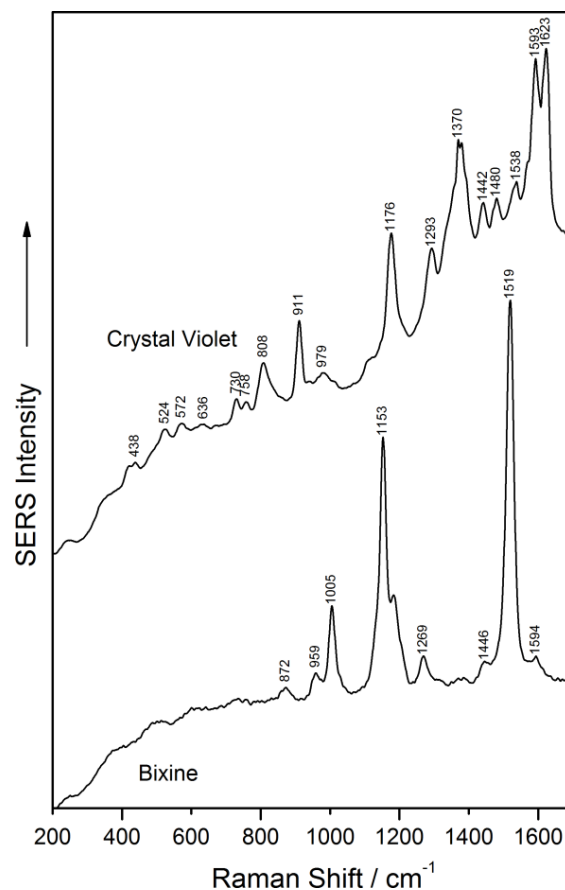

Fig.16. SERS spectra of crystal violet and bixine recorded after a separation of their binary mixture on the AgNO₃ pretreated TLC plate.

Polyethylene glycol synthesized gold nanoparticles

SERS colloidal substrates have a variety of applications that usually depend on their size, distribution [118], stability [119], etc. Frens showed that by using different concentrations of the metal salt solution or by changing the rates of the nucleation and growth of metal particles processes during the synthesis of the metal particles, one can obtain specific sized NPs [118]. Analyzing the coagulation concentration for silver and gold sols in different conditions, the same author concluded that the stability of the colloidal suspensions depends on the NPs diameter [119]. A special attention was paid to the investigation of the optical absorption spectra of silver or gold NPs with the aim of reaching higher SERS enhancement factors. In colloidal suspensions, the well-defined nanostructures must have certain dispersion, size and shape since their optical properties highly depend on these features [120]. In addition, it is a fact that silver

is much more efficient as optical enhancer and for same particle size and shape it yields EFs of 2 or 3 orders of magnitude larger than those of gold [121]. Besides the influence of the temperature, ionic strength and aggregation behavior, the colloids are strongly affected by chloride ions [122] and pH values [123]. Gold and silver are intrinsically good catalysts for different types of reactions: photoreduction, photodecomposition, photoisomerization, etc. In these cases, photocatalytic changes can be induced in the analyte, especially when the SERS spectrum cannot be explained on the basis of the Raman spectrum.

Important characteristics of the colloidal solutions include ease of preparation, reproducibility, stability, compatibility with biomolecules and the important ability to tune the electromagnetic characteristics of the surface by controlling particle size. The versatility of this approach is a promising development for analytical applications. Turkevich et al. [124] studied various preparations methods of colloidal gold: Faraday sol [125], acetone sol, tannin sol [126], oxalic acid sol, hydroxylamine sol [127], Donau sol [128], acetylene sol, citric acid sol, sodium citrate sol etc . The conventional gold colloid is obtained by citrate reduction because of its high SERS activity.

Here, we report a very effective, simple, one step and rapid synthesis method for stable, highly surface-enhanced Raman scattering (SERS) active gold colloids, by reduction and stabilization with short and long chain polyethylene glycol, PEG200 and PEG8000, respectively. Depending on the mixing rate during the synthesis, the mean size of the GNPs can be controlled between 15 and 60 nm. UV-Vis spectra of the synthesized colloids provide information about the diameter and the stability of the PEG synthesized GNPs. According to Haiss et al. [129] the diameter of GNPs can be calculated by using the ratio of the absorbance of GNPs at the plasma resonance peak (A_{SPR}) to the absorbance at 450 nm A_{SPR}/A_{450} as shown in Table 6, if the NPs are spherical and uncoated.
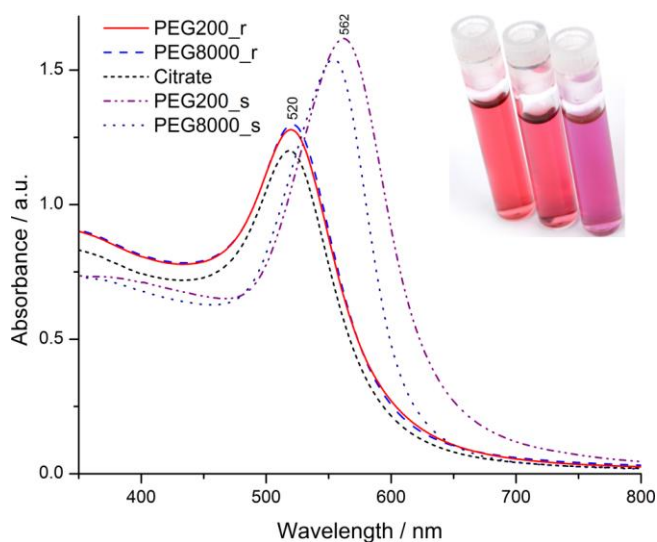

Fig.17. Absorbance spectra of the PEG-coated GNPs in comparison with the citrate reduced GNPs.

$$d = A_{SPR}/ A_{450} \text{ [nm]}$$

Figure 17 shows the UV-vis absorbance spectra of the prepared PEG-coated gold NPs ("_r" means the rapid synthesis method and "_s" means the slow - drop by drop- synthesis method) in comparison with the citrate reduced GNPs. For spherical GNPs an absorption maximum at ~535 nm was expected [130]. However, it was noticed a red shift of the absorption maximum for the slowly reduced gold colloidal solution (562 nm). When the rapid method of synthesis is used, the diameter of the obtained GNPs is close to 15 nm, as in the case of citrate reduced GNPs. Figure 18
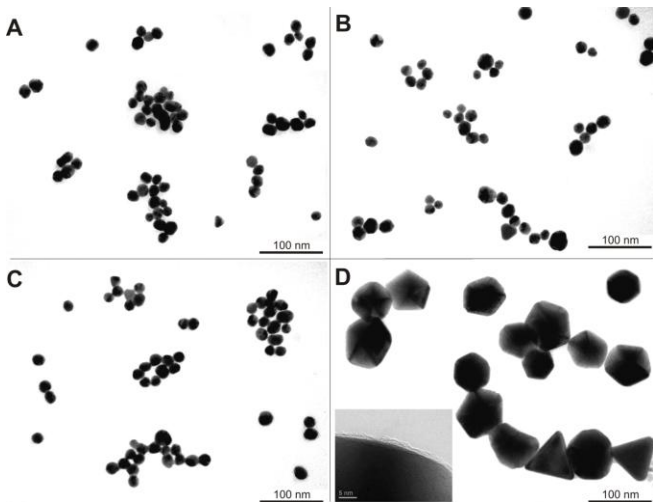
Fig.18. TEM micrographs of the colloidal GNPs PEG200_r (A), PEG8000_r (B), Citrate (C) and PEG200_s (D) with the absorption spectra shown in Fig.17. The inset presents a high resolution TEM micrograph of a GNP from colloid PEG200_s, showing a 2-3 nm PEG layer on the GNP surface.

presents the TEM micrographs (micrograph A and B) of the PEG200 and PEG8000 rapidly reduced colloids show preponderant spherical NPs, with a mean diameter of 15 nm. A dropwise addition of the gold salt to the reaction mixture probably leads to a seeding effect, resulting in a growth of the GNPs. A slow reduction process of the gold salt leads to a gold colloidal solution with an absorption maximum at 562 and 554 nm, when using PEG200 and PEG8000, respectively.

The PEG cover of the GNPs acts as stabilizer, avoiding particles aggregation, leading thus to the high stability of the gold colloid, over months. However, the PEG coating of the GNPs does not induce a shift larger than 2 nm in the UV-Vis spectra [129].

Figure 19 shows the absorption maximum of colloids which blue shifts with the increasing of the PEG200 amount added during the synthesis process. Dynamic light scattering offers important information of the NPs size and the size distribution of the PEGylated GNPs. Figure 20 shows the size distribution of the PEG200 coated GNPs of different sizes. It can be observed that the studied NPs have the diameter around 90 nm (PEG200_s) and 11-18 nm (PEG200_r).
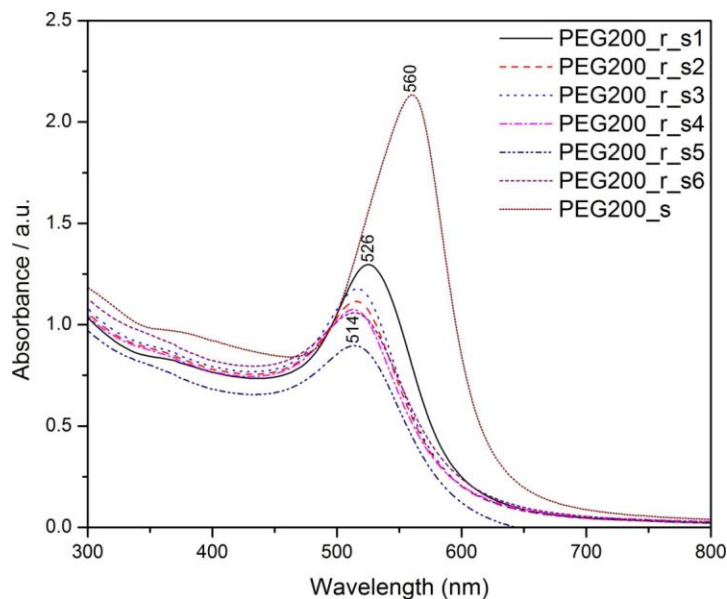

Fig.19. UV-Vis absorption spectra of the colloidal solution obtained by adding different amounts of PEG200, rapidly (PEG200_r) reduced, and drop by drop, therefore slowly (PEG200_s) reduced.

29

The next purpose was to find which one of the PEG synthesized colloids is the most stable. The stability of the colloidal solution is important because it makes them suitable for SERS measurements. Figure 21 shows the stability of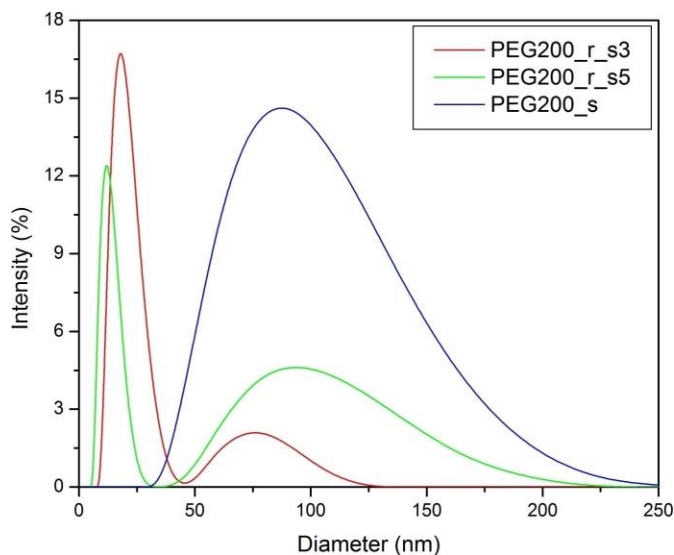 the colloids reduced with short chain PEG. Zeta potential value between 40 and 60 mV indicates a good stability. It can be deduced that the colloid with large NPs (>30 nm) is more stable (a Zeta potential value around -60 mV) than the colloidal solution with small NPs (NPs with a diameter lower than 30 nm show a Zeta potential value around -40 mV). The Zeta potential measurements also show that the layer of PEG which covers the GNPs is negatively charged.

Conclusively, a new, effective and simple procedure for preparing stable, highly SERS-active gold colloids based on reduction and stabilization with short and long chain PEG has been described.

Fig.20. The size distribution of the PEG200 coated GNPs of different sizes.

Depending on the mixing rate of the two reagent solutions, different average particle diameters (between 15 and 60 nm) can be obtained. TEM micrographs of the PEG reduced gold colloids show that the GNPs are predominantly spherical for the 15 nm particles and polygonal for the 60 nm GNPs, respectively.

The significantly cheaper, simpler, more reproducible and faster accomplishment renders this new synthesis method advantageous, compared to the GNPs PEGylation procedures reported in the literature [131-132].
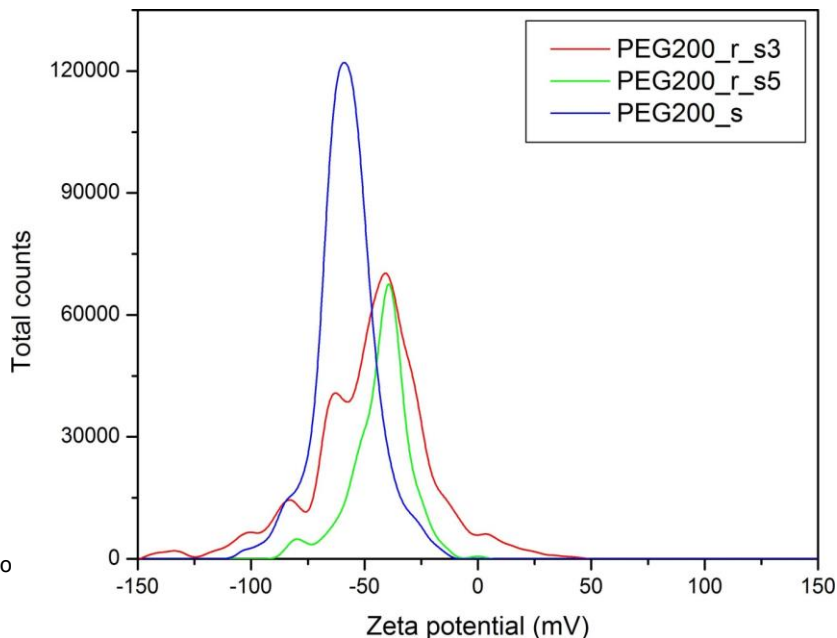
Fig.21. The Zeta potential measurements of different sizes o PEG200 coated GNPs.

30

SERS-based detection of UTI pathogens

Urinary tract infections (UTIs) refer to the presence of microbial pathogens within the urinary tract. Testing for the existence of microorganisms in urine samples in order to diagnose UTIs, which are considered the most commonly acquired bacterial infections, is a routine medical procedure. *E. coli* remains a more common uropathogen, in addition to enterococci, *Pseudomonas*, and *Proteus mirabilis*.

Currently, UTIs can be diagnosed by using the urine dipsticks that can detect the presence of leukocytes esterase, a marker for white blood cells, therefore an indicator of an infection. Since it fails to detect the Gram-positive bacteria, this test has about 68%-88% sensitivity [39]. The alternative available tests rely on more complex methods, like nucleic acid-based polymerase chain reaction (PCR), enzyme-linked immunosorbent assay (ELISA) [40] and matrix-assisted laser desorption/ionization (MALDI) [41-42], which all require an actual culture of the pathogens to test on. The cultivation step is costly and time-consuming and unfortunately, the urine dipstick, as the only cheap and fast test, needs almost always a confirmation. PCR and capture antibody-based sandwich immunoassay [43] have several potential problems, such as high rate of false negatives and false positives. Different recent approaches that possess a high sensitivity are molecular techniques, such as fluorescence in situ hybridization (FISH) [44] or loop-mediated isothermal amplification (LAMP) [45], being also used to identify UTI causative pathogens. In these cases, the sample preparation and post-processing fluorescence imaging make them difficult, complicated and relying on highly skilled personnel.

Therefore, there is a growing need to ensure appropriate and fast diagnosis, succeeded by further investigation to estimate the risk of developing an antimicrobial resistance. Vibrational spectroscopy is a powerful tool considering the high and well-defined spectral information and the simple, mobile and cheap equipment required. Raman spectroscopy is the most promising due to its speed, versatility, minimum sample preparation steps and low-cost instrumentation. Raman spectra could be used for identification and classification of microorganisms once a procedure with good reproducibility and reliability is established. However, the spontaneous Raman effect is so weak that fluorescence, when it occurs, obscures the Raman spectrum. In order to overcome this inconvenient effect, SERS is successfully employed while it suppresses fluorescence and greatly increases the Raman signal. SERS, by its nature of enhancing the Raman cross-sections, provides intense spectra, allowing the detection down to the single (bio)molecule level [133-135]. Moreover, SERS provides reduced spectral recording time and therefore allows the recording of significant number of spectra for a reliable statistic model in a short time. SERS is nowadays a well-established ultrasensitive technique with a high potential of tackling the issues of analytical chemistry and biosciences, even if it requires a great effort of understanding the enhanced vibrational spectrum and still relies on the vibrational patterns identification.

UTI diagnosis is a multistep process which includes the determination of the pathogen concentration, the identification of the responsible bacteria strain as well as its susceptibility to various antibiotics, the so-called antibiogram. Such assays require repeated culturing of the sample and are usually done within 48 h. Moreover, this procedure has other short term and long term consequences, like the unsuccessful treatment of the infection- leading to chronic stage- and the increased antibiotics resistance by a growing number of bacterial strains [136-137].

In this study, we first investigated the optimum conditions for maximum Raman signal enhancement and acquisition of more detailed SERS spectra by influencing the particle surface charges by varying the pH of the sample and by using silver NPs with different surface charges. Then we increased the concentration of the colloidal silver solution at the predetermined experimental conditions to increase the possibility of acquiring reproducible SERS spectra by increasing the density of the silver NPs in the sample.

SERS detection of UTI pathogens biomass

We evaluated the SERS detection of single-bacterium from a monolayer of bacteria adsorbed on a modified glass substrate. The hypothesis that we were aiming to proof is the possibility to reproducibly identify *E. coli,* by SERS, independently of O-type antigen, strain and growth phase. For this purpose, we firstly optimized the experimental conditions for a maximum reproducibility, best Raman signal enhancement and a detailed SERS spectra acquisition without inducing the photo bleaching effect. The main variables during the SERS spectra acquisition were the evaporation-induced reorientation of the molecules, in order to generate a charge-coupling between the microorganisms and the metallic surface (wet and dry conditions) and the careful adjustment of the laser power and of the integration time in order to avoid the local heating of the metallic NPs and consequently, the photo dissociation of the microorganisms situated at SERS hot spots [138].

First of all we proved the bacteria fixation on the unspecific glass substrate for further recording SERS spectra of bacterial biomass. For this purpose, the biomass was applied on the positively charged glass surface, followed by a washing step with Millipore water, to ensure that only a bacterial monolayer is immobilized on the surface. Next, a two-step synthesis of the SERS-active substrate, as reported by Efrima et al. [48] was carried out. Briefly, a silver nitrate solution was added and let to adhere (1 h), and then the hydroxylamine hydrochloride reducing agent, was added (1 h action time). After several hours, coalescence of silver clusters was observed, as silver islands (dark spots), still attached on the glass surface after another washing step. These silver islands provided the most enhanced Raman spectra, acting thus as SERS substrate. When using this two-step synthesis but in a simple mixture with the bacterial solution, the bacteria were covered by the Ag NPs as described in the schematic view of the synthesis procedure included in Figure 22.
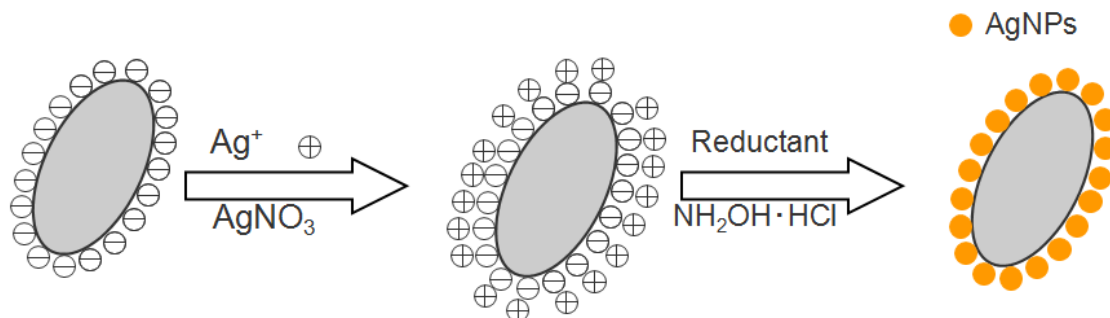
In situ 2-step-synthesis of Silver NPs

Fig.22. Schematic view of the two-step synthesis of Ag NPs.

Figure 23 shows the TEM micrographs obtained from the mixture of Ag NPs synthesized as described above and the bacterial suspension. In the left image the bacteria were not mixed with NPs and in the right image can be observed how the Ag NPs cover the bacterial cell wall, forming clusters by aggregation.
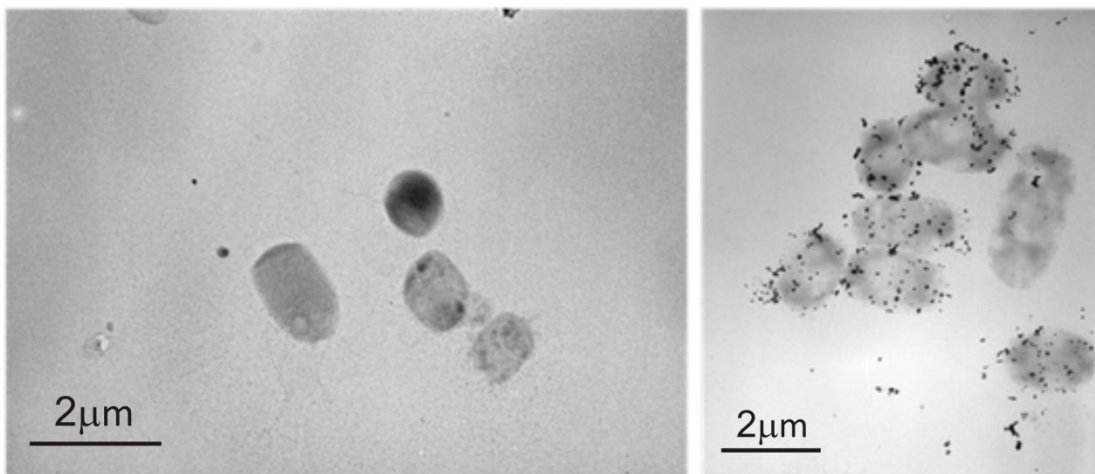
Fig.23. TEM micrographs obtained on the bacteria (left) and also on the mixture of bacteria with Ag NPs (right).

Figure 24 shows SERS spectra recorded by focusing the 633 nm laser on such silver clusters which are in the close proximity of the bacterial biomass. The inset in Figure 24 shows the biomass of one rough *E. coli* strain (*DSM 1116*) captured on the glass substrate. Also, several silver clusters can be observed in the inset image. Mainly, the SERS bands are assigned to the cell wall fingerprint: the glycosidic ring deformation vibration at 554 cm^{-1} and 749 cm^{-1}, the phospholipids C-C skeletal vibration at 889 cm^{-1}, the amide III band at 1242 cm^{-1} and, the CH$_2$ deformation at 1465 cm^{-1}. In the higher wavenumbers region, the most intense Raman bands are at 1287 cm^{-1} and 1358 cm^{-1}, ascribed to the CH deformations in proteins. These putative assignments rely heavily on previous studies and are included in Table 4.
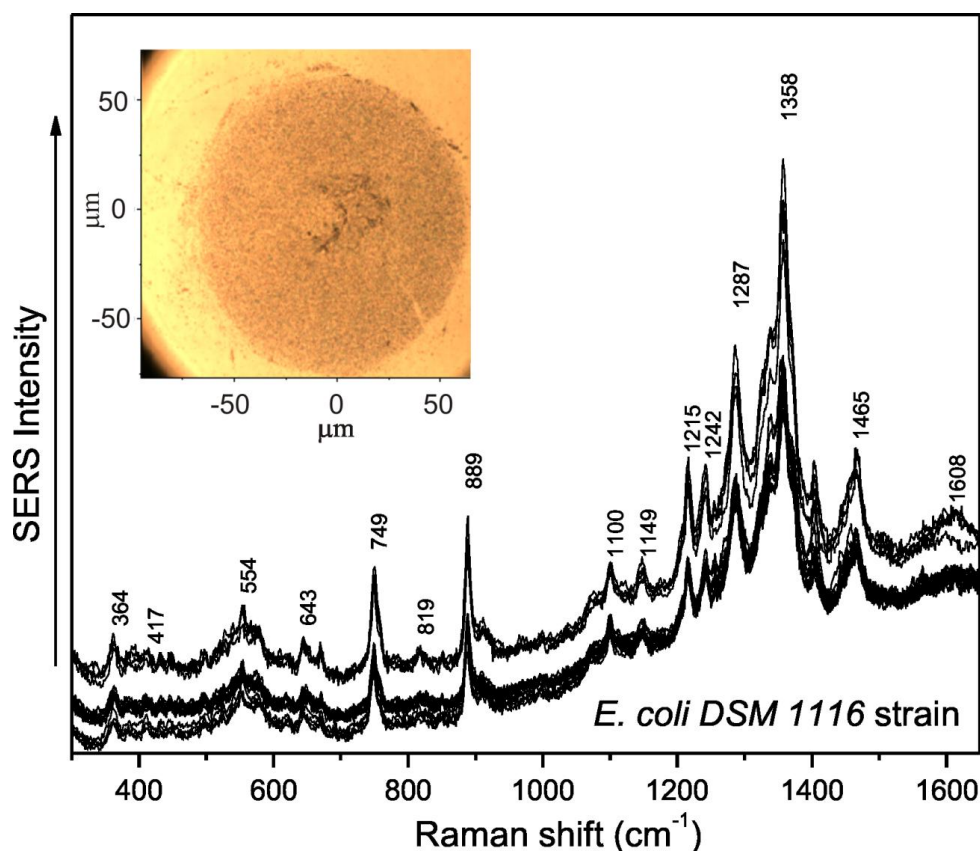
Fig.24. SERS spectra collected from the E. coli DSM 1116 biomass after electrostatic immobilization and in situ silver substrate preparation. Inset,-microscopic 50x objective image of the tested E. coli DSM 1116 biomass.

Table 4. Tentative assignments of the SERS spectra of the characterized bacteria.

Wavenumbers(cm^{-1})	Band assignments	References
364-474	Carbohydrates	[139]
500-586	Carbohydrates, Glycosidic ring	[140]
643-688	δ(COO$^-$), Guanine	[35, 141]
721-749	Glycosidic ring, Adenine	[139, 142-143]
801-819	Out-of-plane ring breathing tyrosin	[144]
867-889	C-O-C ring deformation	[144]
921-953	Ring breathing vibration	[145]
1100-1130	δ(CC,CO,-COH) carbohydrates	[33]
1149-1209	=C-C= lipid	[139]
1242-1245	Amide III	[141]
1266-1287	δ(CH) protein	[141]
1346-1368	δ(CH) protein	[146]
1422-1465	δ(CH$_2$) saturated lipids	[142]
1523-1543	Ring stretching vibration	[145]
1589-1668	ν(DNA)	[142]
1690-1702	ν(C=C)	[145]

SERS detection at single-bacterium level

Using the following approach we were able to reduce the sample preparation time to less than 2 h, and also to record single-bacterium SERS spectra. We have previously clarified the advantages of using the concentrated AgNPs [54]. By using a 4 times concentrated solution of silver NPs (described in the preparation of concentrated silver NPs section), SERS spectra were collected after several minutes of incubation. In this experimental procedure, the biomass harvested from an overnight culture was applied on the glass surface and left to adsorb for 30 min, then the glass slide was washed. The 4 times concentrated colloidal suspension was added on the freshly washed glass slide and after another 30 min the bacteria attached on the glass surface were Raman tested. This way we considerably reduced the analysis time to less than 2h. By using the 100x objective, we could confirm the immobilization of single bacterial cells, isolated, as well as in silver islands. SERS spectra were collected only from single cell events and some representative results for each strain in stationary phase are shown in Figure 25. The inset in Figure 25 shows a microscopic view of isolated single *E. coli* bacteria tested by the aforementioned procedure. The spectra were normalized and the baseline was subtracted for a clear visualization.
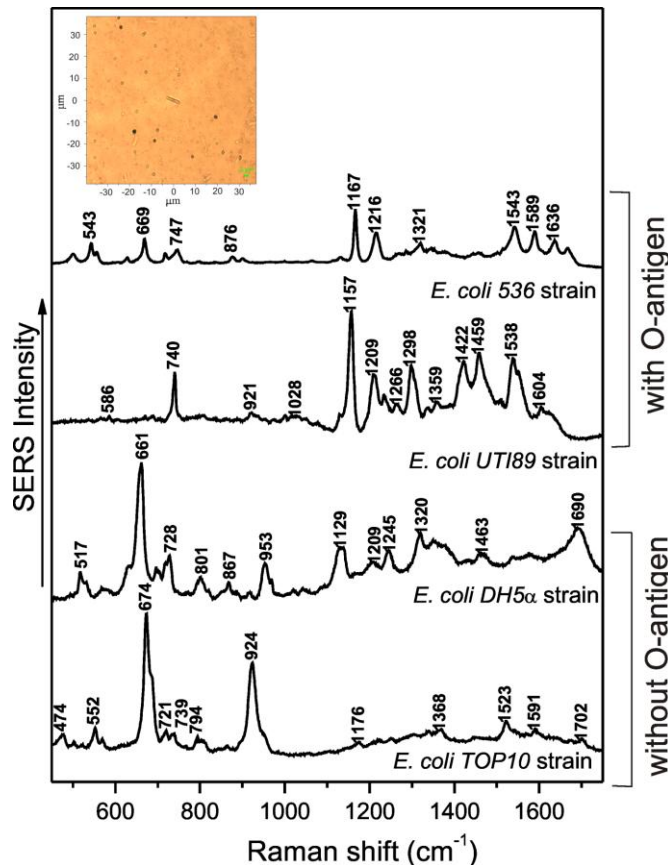
The presence of the O-antigen influences significantly the SERS spectral features. As far as we can conclude from the SERS spectra resulted by using the concentrated silver NPs, the enhanced Raman bands belong to the glycosidic ring and aromatic ring breathing vibrations in the case of rough *E. coli* strains (without the O-antigen). For the smooth strains, with O-antigen, the dominant spectral features are due to the glycosidic ring and to the (=C-C=) lipids, δ(CH) proteins and amide III vibrations. However, the most prevalent molecules that could interact with the silver metal surface are amino acids, proteins, lipids and sugars.

Fig.25. Single-bacterium SERS spectra of rough strains (without O-antigen: *DH5a* and *TOP10*), and of smooth strains (with O-Antigen: *UTI89*, *536*), respectively. Inset- microscopic image of the tested *E. coli DH5a rough strain.*

SERS investigation of single-bacterium in different growth phases

Because in the case of an infection, one can expect bacteria in different growth phases in the urine sample, we decided to test the developed SERS detection approach for single-bacterium in two growth phases. For this purpose, we used a stationary phase culture (overnight cultivation time) and a mid-log phase culture (3h cultivation time). The tested samples had bacterial biomass in concentrations between 10^5 and 10^7cells/ml, comparable to those determined in the real UTIs cases. By using the approach optimized for single-bacterium detection, SERS spectra were recorded from two different strains of *E. coli*, as shown in Figure 26(a rough strain-*DH5a,* Figure 26A and a smooth strain-*536,* Figure 26 B), from mid-log growth phase bacterial cultures. By comparing the repetitive single-bacterium SERS spectra acquired for each *E. coli* strain in mid-log growth phase (Figure 26), slight modifications in band positions and relative intensities can be observed. For instance, the band at 723 cm^{-1}, ascribed to the glycosidic ring vibration, is shifted to 726 cm^{-1} or even to 738 cm^{-1}. In the case of *E. coli DH5a* rough strain for the stationary phase (Figure 25) the marker band with the highest intensity is the specific guanine band at 661 cm^{-1}, while for the mid-log phase the highest band is the one specific to the glycosidic ring vibration in the range of 723-738 cm^{-1}. In the case of *E. coli 536* smooth strain, the most intense band is at 1167 cm^{-1} for the stationary phase, whereas for the mid-log phase the SERS spectrum is dominated by the band at 580 cm^{-1}, specific to carbohydrates.
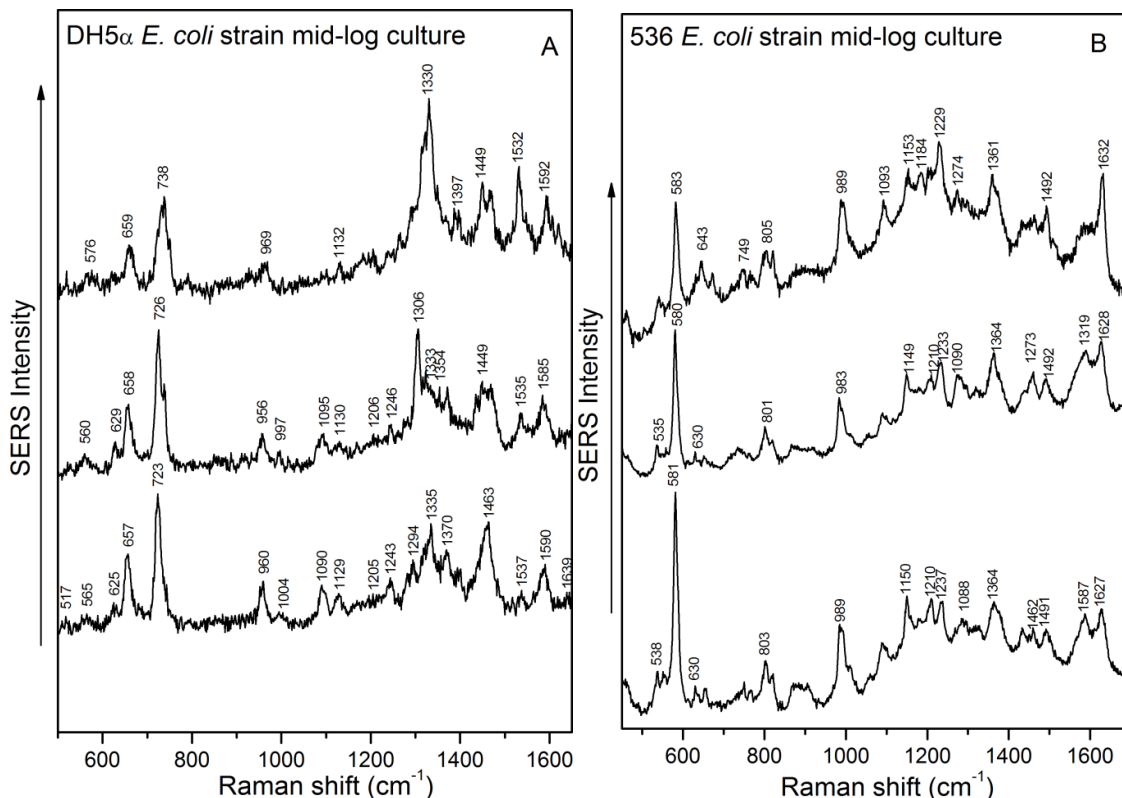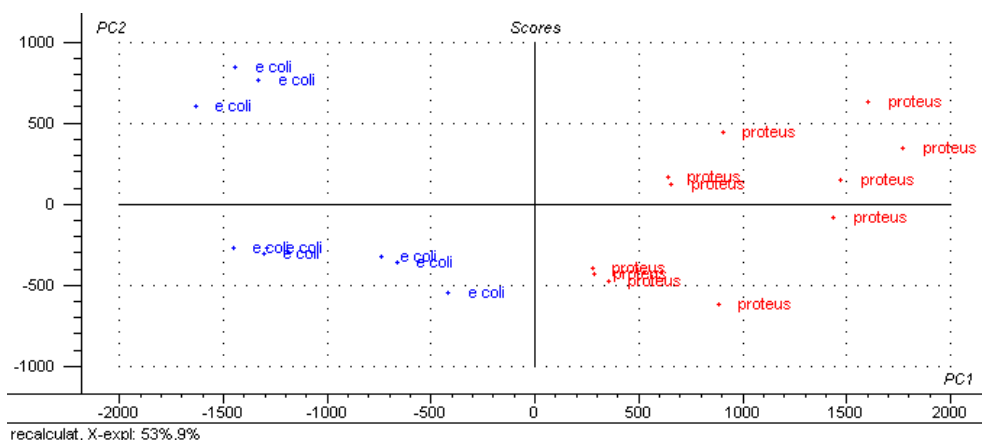

Fig.26. SERS spectra collected from three different single-bacterium of *DH5a rough strain* (A) and of *536 smooth strain* (B) in mid-log growth phase, respectively.

UTI pathogens discrimination by PCA analysis based on the SERS spectra

For obtaining the configuration and the composition of the outer membrane layer, an analysis that combines chromatographic and spectroscopic techniques is required. The essential information from complex spectroscopic patterns is usually extracted by using pattern recognition techniques, like chemometrics. In order to assess the identification potential of the single-bacterium SERS spectra, principal component analysis (PCA) was performed on the unprocessed single-bacterium SERS spectra collected from two different microorganisms (*E. coli* and *P. mirabilis*), harvested in the stationary phase.

PCA is a common multicomponent analysis method used to find the main variance sources in data sets. We used the software Unscrambler X 10.0 (CAMO Software, Norway) to perform the PCA analysis (full cross validation computation model, preprocessing by eliminating the scattering effect present as background in all 19 spectra) on the single-bacterium SERS spectra. The highest variance in the spectral features was shown by the first two components scores. These results plotted explain 60% of the spectral differences present in the 650-1650 wavenumbers region, considered as the spectral bacterial fingerprint. From the loadings chart, it can be observed that the highest contribution in discriminating *E. coli* and *P. mirabilis* samples is correlated with the marker Raman bands, at 727 cm^{-1} and 650-675 cm^{-1}, present with different relative intensities in all SERS spectra. Figure 27 fairly discriminates between two groups of SERS spectra: one group corresponds to the *E. coli DH5α·* and the second one to the *P. mirabilis.* Conclusively, by using unbiased computational resources, by means of principal component analysis, two of the most common UTI pathogens were discriminated.

Obtaining reproducible SERS spectra is crucial for accurate bacterial identification at strain level in real-life applications. The common labor-intensive procedure of detecting the type of microorganism that causes an infection at strain level and also which could be the effective antibiotic against it can last 1-3 days for a full result. By using a SERS-based approach, a valuable input can be provided to the clinician in several hours.

Fig.27. PCA scores showing the two separated groups: *E. coli* (blue, "*e coli*") and *P. mirabilis* (red, "proteus").

Conclusions

The aim of this thesis was to employ theoretical and spectroscopic techniques and to develop new SERS-based biomedical applications in order to investigate chemical entities with relevant pharmaceutical or food control use and pathogenic microorganisms. The main achieved objectives are summarized here.

In the first part of the scientific results included in this thesis, a theoretical and vibrational analysis of nitrogen-rich biomedical compounds was assessed. The complex investigation revealed the vibrational behavior of melamine and zidovudine and also predicted the mechanism of adsorption on the silver surface, the SERS-active substrate used for the trace level detection. The obtained LODs are in the required range for monitoring food control aspects on different milk products (in the case of melamine) and also in terms of pharmaceutical toxicology and treatment efficiency (for zidovudine).

The second part was focused on the development of new SERS-active substrates for ultrasensitive detection. For this purpose, SERS was coupled with TLC in order to test Ag NPs synthesized by laser-induced reduction of a silver salt in the presence of different chromophores. The separation of binary mixtures was achieved by using TLC plates pretreated with the silver salt in order to enable the Ag reduction by laser exposure. The results confirmed that this new technique can be employed successfully in the ultrasensitive detection of analytes forming binary mixtures. Another new SERS-active substrate was synthesized by using biocompatible polymers as reducing agent for gold salts. This technique allows the synthesis of different sized-NPs depending on the amount and the rate of addition of the polymer during the reducing reaction. Spectroscopic techniques as SERS, UV-VIS and DLS were used for the characterization of the new PEG-reduced GNPs.

The last part of scientific results describes a SERS-based detection methodology for UTI pathogens at single-bacterium level. The novelty of this approach consists in using exclusively electrostatic forces for bacteria immobilization on the glass slide. The reduced analysis time and the possibility of discriminating between different types of microorganisms or different strains of the same type of pathogen by using PCA analysis are the main advantages of the detection method proposed in this work. We systemically investigated the potential origins of the vibrational features in the bacterial SERS recorded spectra. We are confident that these results motivate the potential routine practice for a large number of samples because of the straightforward sample preparation and detection procedure and the minimum reagent usage and costs. This way we would avoid the common clinical practice of administrating a broad-spectrum antimicrobial therapy that could induce a drug resistance in time and the clinician could target an efficient therapy to the specific UTI causative pathogen. The obtained data set enabled us to draw the following important conclusions: this study could provide the reliable and fast answer needed to enable a quick UTI diagnosis due to the observed spectral differences between growth phases, strains and types of Gram-negative microorganisms.

References

1. Kruszewska, H., et al., *Spectroscopic identification of AZT derivative obtained from biotransformation of AZT by Stenotrophomonas maltophilia.* Journal of Molecular Structure (2003) **651–653**:0, 645-650.
2. Raviolo, M.A., J. Esteve-Romero, and M.C. Briñón, *Stability-indicating micellar liquid chromatography method for three novel derivatives of zidovudine in aqueous and simulated gastric and intestinal fluids matrices.* Journal of Chromatography A (2011) **1218**:18, 2540-2545.
3. Dunge, A., et al., *Validated specific HPLC method for determination of zidovudine during stability studies.* Journal of Pharmaceutical and Biomedical Analysis (2005) **37**:5, 1109-1114.
4. Ramachandran, G., et al., *A simple and rapid liquid chromatography method for simultaneous determination of zidovudine and nevirapine in plasma.* Journal of Chromatography B (2006) **843**:2, 339-344.
5. Breidbach, A., et al., *Capabilities of laboratories to determine melamine in food-results of an international proficiency test.* Analytical and Bioanalytical Chemistry (2010) **396**:1, 503-510.
6. *Melamine: Information for Pediatric Health Professionals PEHSU (Pediatric Environmental Health Specialty Units)*. 8 January 2009.
7. Lin, M., et al., *Detection of Melamine in Gluten, Chicken Feed, and Processed Foods Using Surface Enhanced Raman Spectroscopy and HPLC.* Journal of Food Science (2008) **73**:8, T129-T134.
8. Huang, H., et al., *Surface-enhanced Raman spectra of melamine and other chemicals using a 1550 nm (retina-safe) laser.* Journal of Raman Spectroscopy (2012) **43**:6, 701-705.
9. Zhang, B., et al., *Acid-directed synthesis of SERS-active hierarchical assemblies of silver nanostructures.* Journal of Materials Chemistry (2011) **21**:8, 2495-2501.
10. Chen, L., et al., *ZnO/Au Composite Nanoarrays As Substrates for Surface-Enhanced Raman Scattering Detection.* The Journal of Physical Chemistry C (2009) **114**:1, 93-100.
11. Lee, S.Y., et al., *Detection of Melamine in Powdered Milk Using Surface-Enhanced Raman Scattering with No Pretreatment.* Analytical Letters (2010) **43**:14, 2135-2141.
12. Zhang, X.F., et al., *Detection of melamine in liquid milk using surface-enhanced Raman scattering spectroscopy.* Journal of Raman Spectroscopy (2010) **41**:12, 1655-1660.
13. Zhang, J., et al., *Quantitative surface enhanced Raman scattering detection based on the "sandwich" structure substrate.* Spectrochim Acta A Mol Biomol Spectrosc (2011) **79**:3, 625-30.
14. Mircescu, N.E., et al., *FTIR, FT-Raman, SERS and DFT study on melamine.* Vibrational Spectroscopy (2012) **62**:0, 165-171.
15. Zhou, F.X., et al., *Radiosensitization effect of zidovudine on human malignant glioma cells.* Biochemical and Biophysical Research Communications (2007) **354**:2, 351-356.
16. Rivas, L., S. Sanchez-Cortes, and J.V. García-Ramos, *Conformational study of AZT in aqueous solution and adsorbed on a silver surface by means of Raman spectroscopy.* Journal of Raman Spectroscopy (2002) **33**:1, 6-9.
17. Kumakura, A., et al., *Polarized Raman spectrum of a single crystal of AZT.* Biospectroscopy (1996) **2**:4, 233-242.
18. Mircescu, N.E., et al., *Surface-enhanced Raman and DFT study on zidovudine.* Spectroscopy (2011) **26**:4-5, 311-315.
19. Raviolo, M.A., et al., *Synthesis, molecular structure and physicochemical properties of bis(3'-azido-3'-deoxythymidin-5'-yl) carbonate.* Journal of Molecular Structure (2010) **970**:1–3, 59-65.

20.   Chen, F.-F. and F. Wang, *Electronic Structure of the Azide Group in 3'-Azido-3'-deoxythymidine (AZT) Compared to Small Azide Compounds.* Molecules (2009) **14**:7, 2656-2668.

21.   Ciuffo, G.M., et al., *AZT and related compounds—a theoretical study.* Journal of Molecular Structure: THEOCHEM (1998) **428**:1–3, 155-165.

22.   Mura, M., N. Martsinovich, and L. Kantorovich, *Theoretical study of melamine superstructures and their interaction with the Au(111) surface.* Nanotechnology (2008) **19**:46, 465704.

23.   Drozd, M. and M.K. Marchewka, *The structure, vibrational spectra and non-linear optical properties of neutral melamine and singly, doubly and triply protonated melaminium cations-theoretical studies.* Journal of Molecular Structure-Theochem (2005) **716** 175-192.

24.   Jang, Y.H., et al., *Acid Dissociation Constants of Melamine Derivatives from Density Functional Theory Calculations.* Journal of Physical Chemistry A (2009) **113**:46, 13036-13040.

25.   Sklenák, Š., A. Gatial, and S. Biskupič, *Ab initio study of small organic azides.* Journal of Molecular Structure: THEOCHEM (1997) **397**:1–3, 249-262.

26.   Hai-ling, X., Z. Ru-gang, and Z. Da-wei. *Analytical System Based on Raman Spectroscopy in Melamine Detection*. in *Biomedical Engineering and Informatics, 2009. BMEI '09. 2nd International Conference on*. 2009.

27.   Hu, H., et al., *Ag-Coated Fe3O4@SiO2 Three-Ply Composite Microspheres: Synthesis, Characterization, and Application in Detecting Melamine with Their Surface-Enhanced Raman Scattering.* The Journal of Physical Chemistry C (2010) **114**:17, 7738-7742.

28.   He, L., et al., *A new approach to measure melamine, cyanuric acid, and melamine cyanurate using surface enhanced Raman spectroscopy coupled with gold nanosubstrates.* Sensing and Instrumentation for Food Quality and Safety (2008) **2**:1, 66-71.

29.   Wen, Z.-Q., G. Li, and D. Ren, *Detection of Trace Melamine in Raw Materials Used for Protein Pharmaceutical Manufacturing Using Surface-Enhanced Raman Spectroscopy (SERS) with Gold Nanoparticles.* Appl. Spectrosc. (2011) **65**:5, 514-521.

30.   Du, X., et al., *Qualitative and Quantitative Determination of Melamine by Surface-Enhanced Raman Spectroscopy Using Silver Nanorod Array Substrates.* Appl. Spectrosc. (2010) **64**:7, 781-785.

31.   Lou, T., et al., *Rapid detection of melamine with 4-mercaptopyridine-modified gold nanoparticles by surface-enhanced Raman scaterring.* Analytical and Bioanalytical Chemistry (2011).

32.   Cheng, Y., et al., *Screening melamine adulterant in milk powder with laser Raman spectrometry.* Journal of Food Composition and Analysis (2010) **23**:2, 199-202.

33.   Schuster, K.C., et al., *Multidimensional Information on the Chemical Composition of Single Bacterial Cells by Confocal Raman Microspectroscopy.* Analytical Chemistry (2000) **72**:22, 5529-5534.

34.   Schuster, K.C., E. Urlaub, and J.R. Gapes, *Single-cell analysis of bacteria by Raman microscopy: spectral information on the chemical composition of cells and on the heterogeneity in a culture.* Journal of Microbiological Methods (2000) **42**:1, 29-38.

35.   Knauer, M., et al., *Surface-Enhanced Raman Scattering-Based Label-Free Microarray Readout for the Detection of Microorganisms.* Analytical Chemistry (2010) **82**:7, 2766-2772.

36.   Knauer, M., et al., *A flow-through microarray cell for the online SERS detection of antibody-captured E. coli bacteria.* Analytical and Bioanalytical Chemistry (2012) **402**:8, 2663-2667.

37.   Foxman, B., *Epidemiology of urinary tract infections: Incidence, morbidity, and economic costs.* American Journal of Medicine (2002) **113** 5S-13S.

38.   Foxman, B., *Epidemiology of urinary tract infections: Incidence, morbidity, and economic costs.* Dm Disease-a-Month (2003) **49**:2, 53-70.

39.   Deville, W., et al., *The urine dipstick test useful to rule out infections. A meta-analysis of the accuracy.* BMC Urology (2004) **4**:1, 4.

40.   Guven, B., et al., *SERS-based sandwich immunoassay using antibody coated magnetic nanoparticles for Escherichia coli enumeration.* Analyst (2011) **136**:4, 740-748.

41.   Wieser, A., et al., *MALDI-TOF MS in microbiological diagnostics-identification of microorganisms and beyond (mini review).* Appl Microbiol Biotechnol (2012) **93**:3, 965-974.

42.   Sören, S.S., et al., *Novel, improved sample preparation for rapid, direct identification from positive blood cultures using matrix-assisted laser desorption/ionization time-of-flight (MALDI-TOF) mass spectrometry.* J Mol Diagn (2011) **13**:6, 701-706.

43.   Langer, V., R. Niessner, and M. Seidel, *Stopped-flow microarray immunoassay for detection of viable E. coli by use of chemiluminescence flow-through microarrays.* Analytical and Bioanalytical Chemistry (2011) **399**:3, 1041-1050.

44.   Wu, Q., et al., *Fluorescence in situ hybridization rapidly detects three different pathogenic bacteria in urinary tract infection samples.* Journal of Microbiological Methods (2010) **83**:2, 175-178.

45.   Safavieh, M., et al., *Microfluidic electrochemical assay for rapid detection and quantification of Escherichia coli.* Biosensors and Bioelectronics (2012) **31**:1, 523-528.

46.   Zeiri, L., et al., *Surface-enhanced Raman spectroscopy as a tool for probing specific biochemical components in bacteria.* Appl Spectrosc (2004) **58**:1, 33-40.

47.   Sengupta, A., M. Mujacic, and E.J. Davis, *Detection of bacteria by surface-enhanced Raman spectroscopy.* Analytical and Bioanalytical Chemistry (2006) **386**:5, 1379-1386.

48.   Efrima, S. and B.V. Bronk, *Silver Colloids Impregnating or Coating Bacteria.* Journal of Physical Chemistry B (1998) **102**:31, 5947-5950.

49.   Knauer, M., et al., *Optimized surface-enhanced Raman scattering (SERS) colloids for the characterization of microorganisms.* Anal Sci (2010) **26**:7, 761-766.

50.   Kim, Y., et al., *Label-free detection of a bacterial pathogen using an immobilized siderophore, deferoxamine.* Lab on a Chip (2012) **12**:5, 971-976.

51.   Doorneweerd, D.D., et al., *Selective Capture and Identification of Pathogenic Bacteria Using an Immobilized Siderophore.* Langmuir (2010) **26**:19, 15424-15429.

52.   Bugdahn, N., et al., *Direct Identification of a Siderophore Import Protein Using Synthetic Petrobactin Ligands.* Angewandte Chemie International Edition (2010) **49**:52, 10210-10213.

53.   Zheng, T., J.L. Bullock, and E.M. Nolan, *Siderophore-Mediated Cargo Delivery to the Cytoplasm of Escherichia coli and Pseudomonas aeruginosa: Syntheses of Monofunctionalized Enterobactin Scaffolds and Evaluation of Enterobactin-Cargo Conjugate Uptake.* J Am Chem Soc (2012).

54.   Kahraman, M., et al., *Reproducible Surface-Enhanced Raman Scattering Spectra of Bacteria on Aggregated Silver Nanoparticles.* Appl. Spectrosc. (2007) **61**:5, 479-485.

55.   WHO, *Toxicological and health aspects of melamine and cyanuric acid* 2009, World Health Organization: Geneva.

56.   Muñiz-Valencia, R., et al., *Method development and validation for melamine and its derivatives in rice concentrates by liquid chromatography. Application to animal feed samples.* Analytical and Bioanalytical Chemistry (2008) **392** 523-531.

57.   Ibanez, M., J.V. Sancho, and F. Hernandez, *Determination of melamine in milk-based products and other food and beverage products by ion-pair liquid chromatography-tandem mass spectrometry.* Analytica Chimica Acta (2009) **649**:1, 91-97.

58.   Tittlemier, S., *Methods for the analysis of melamine and related compounds in foods: A review.* Food Additives and Contaminants Part A-Chemistry Analysis Control Exposure & Risk Assessment (2010) **27** 129.

59.   Rima, J., et al., *New spectroscopic method for the quantitative determination of melamine using Mannich reaction.* Journal of Food Composition and Analysis (2009) **22**:7-8, 689-693.

60.   Li, L., et al., *Visual detection of melamine in raw milk using gold nanoparticles as colorimetric probe.* Food Chemistry (2010) **122**:3, 895-900.

61.   Wang, J., et al., *Residue analysis of melamine in milk products by micellar electrokinetic capillary chromatography with amperometric detection.* Food Chemistry (2010) **121**:1, 215-219.

62.   Broszat, M., R. Bramer, and B. Spangenberg, *A new method for quantification of melamine in milk by absorption diode-array thin-layer chromatography.* Journal of Planar Chromatography - Modern TLC (2008) **21**:6, 469-470.

63.   Marcott, C., et al., *Mining the Information Content Buried in Infrared and Near-Infrared Band Shapes by Temporal, Spatial, and Other Perturbations.* Applied Spectroscopy (2009) **63**:12, 346A-354A.

64.   Roy Dennington, Todd Keith, and J. Millam, *GaussView*. 2009, Semichem Inc., Shawnee Mission KS.

65.   Varghese, J.N., A.M. O'Connell, and E.N. Maslen, *The X-ray and Neutron Crystal Structure of 2,4,6-Triamino-1,3,5-triazine (Melamine).* Acta Crystallographica Section B-Structural Science (1977) **33** 2102-2108.

66.   Hirt, R.C. and R.G. Schmitt, *Ultraviolet absorption spectra ot derivatives of symmetric triazine—II: Oxo-triazines and their acyclic analogs* Spectrochimica Acta (1958) **12**:2-3, 127-138.

67.   Pekparlak, A., et al., *Theoretical studies of molecular structure and vibrational spectra of melaminium acetate acetic acid solvate monohydrate.* Spectrochimica Acta, Part A: Molecular and Biomolecular Spectroscopy (2010) **77**:3, 696-702.

68.   Creighton, J.A., *Surface Raman electromagnetic enhancement factors for molecules at the surface of small isolated metal spheres: The determination of adsorbate orientation from SERS relative intensities.* Surface Science (1983) **124**:1, 209-219.

69.   Moskovits, M. and J.S. Suh, *Surface selection rules for surface-enhanced Raman spectroscopy: Calculations and application to the surface-enhanced Raman spectrum of phthalazine on silver.* Journal of Physical Chemistry (1984) **88**:23, 5526-5530.

70.   Creighton, J.A., *Selection rules for surface-enhanced Raman spectroscopy*, in *Spectroscopy of Surfaces*, R.J.H. Clark and R.E. Hester, Editors. 1988, Wiley: New York. p. 37-89.

71.   Perez-Then, E., *Newborn treatment with nevirapine plus zidovudine reduces mother-to-child transmission of HIV.* Evidence-based Healthcare (2004) **8**:2, 85-86.

72.   N. Leopold, *Surface-Enhanced Raman Spectroscopy. Selected Applications*. 2009, Cluj-Napoca: Napoca Star.

73.   Checa, A., et al., *Fast determination of pKa values of reverse transcriptase inhibitor drugs for AIDS treatment by using pH-gradient flow-injection analysis and multivariate curve resolution.* Analytica Chimica Acta (2005) **554**:1–2, 177-183.

74.   Chen, F.F. and F. Wang, *Electronic Structure of the Azide Group in 3'-Azido-3'-deoxythymidine (AZT) Compared to Small Azide Compounds.* Molecules (2009) **14**:7, 2656-2668.

75.   M.J. Frisch, et al., *Gaussian 03*. 2003, Gaussian, Inc: Pittsburgh PA.

76.   Chiş, V., et al., *Raman, surface-enhanced Raman scattering and DFT study of para-nitro-aniline.* Vibrational Spectroscopy (2008) **48**:2, 210-214.

77.   Otto, A., et al., *Surface-enhanced Raman scattering.* Journal of Physics: Condensed Matter (1992) **4**:5, 1143.

78.   Wang, C.-H., D.-C. Sun, and X.-H. Xia, *One-step formation of nanostructured gold layers via a galvanic exchange reaction for surface enhancement Raman scattering.* Nanotechnology (2006) **17**:3, 651.

79.   Zhou, Q., et al., *Rapid detection of 2, 3, 3', 4, 4'-pentachlorinated biphenyls by silver nanorods-enhanced Raman spectroscopy.* Physica E: Low-dimensional Systems and Nanostructures (2010) **42**:5, 1717-1720.

80.   Yoon, I., et al., *Single Nanowire on a Film as an Efficient SERS-Active Platform.* Journal of the American Chemical Society (2008) **131**:2, 758-762.

81.   Zhang, L., P. Zhang, and Y. Fang, *An investigation of the surface-enhanced Raman scattering effect from new substrates of several kinds of nanowire arrays.* Journal of Colloid and Interface Science (2007) **311**:2, 502-506.

82.   Zong, R.-L., et al., *Synthesis and Optical Properties of Silver Nanowire Arrays Embedded in Anodic Alumina Membrane.* The Journal of Physical Chemistry B (2004) **108**:43, 16713-16716.

83.   Shen, C., et al., *Monodisperse Noble-Metal Nanoparticles and Their Surface Enhanced Raman Scattering Properties.* Chemistry of Materials (2008) **20**:22, 6939-6944.

84.   Dick, L.A., et al., *Metal Film over Nanosphere (MFON) Electrodes for Surface-Enhanced Raman Spectroscopy (SERS): Improvements in Surface Nanostructure Stability and Suppression of Irreversible Loss.* The Journal of Physical Chemistry B (2001) **106**:4, 853-860.

85.   Taylor, G.W., *Detection and Identification of Dyes on Anglo-Scandinavian Textiles.* Studies in Conservation (1983) **28**:4, 153-160.

86.   Leona, M. and J. Winter, *Fiber optics reflectance spectroscopy: a unique tool for the investigation of Japanese paintings.* Studies in Conservation (2001) **46**:3, 153-162.

87.   Claro, A., et al., *The use of microspectrofluorimetry for the characterization of lake pigments.* Talanta (2008) **74**:4, 922-929.

88.   Clementi, C., et al., *In-situ fluorimetry: A powerful non-invasive diagnostic technique for natural dyes used in artefacts: Part II. Identification of orcein and indigo in Renaissance tapestries.* Spectrochimica Acta Part A: Molecular and Biomolecular Spectroscopy (2009) **71**:5, 2057-2062.

89.   Masschelein-Kleiner, L., *Ancient Binding Media, Varnishes and Adhesives*. 1995, Rome: ICCROM. 118.

90.   Centeno, S.A. and J. Shamir, *Surface enhanced Raman scattering (SERS) and FTIR characterization of the sepia melanin pigment used in works of art.* Journal of Molecular Structure (2008) **873**:1–3, 149-159.

91.   Bruni, S., et al., *The joined use of n.i. spectroscopic analyses – FTIR, Raman, visible reflectance spectrometry and EDXRF – to study drawings and illuminated manuscripts.* Applied Physics A (2008) **92**:1, 103-108.

92.   Bell, I.M., R.J.H. Clark, and P.J. Gibbs, *Raman spectroscopic library of natural and synthetic pigments (pre- ≈ 1850 AD).* Spectrochimica Acta Part A: Molecular and Biomolecular Spectroscopy (1997) **53**:12, 2159-2179.

93.   Vandenabeele, P., et al., *Raman spectroscopic database of azo pigments and application to modern art studies.* Journal of Raman Spectroscopy (2000) **31**:6, 509-517.

94.   Schulte, F., et al., *Raman spectroscopy of synthetic organic pigments used in 20th century works of art.* Journal of Raman Spectroscopy (2008) **39**:10, 1455-1463.

95.   Wustholz, K.L., et al., *Surface-enhanced Raman spectroscopy of dyes: from single molecules to the artists' canvas.* Physical Chemistry Chemical Physics (2009) **11**:34, 7350-7359.

96.   Casadio, F., et al., *Identification of Organic Colorants in Fibers, Paints, and Glazes by Surface Enhanced Raman Spectroscopy.* Accounts of Chemical Research (2010) **43**:6, 782-791.

97.   He, L., M.J. Natan, and C.D. Keating, *Surface-Enhanced Raman Scattering: A Structure-Specific Detection Method for Capillary Electrophoresis.* Analytical Chemistry (2000) **72**:21, 5348-5355.

98.   Seifar, R.M., et al., *Applicability of surface-enhanced resonance Raman scattering for the direct discrimination of ballpoint pen inks.* Analyst (2001) **126**:8, 1418-1422.

99.   Soper, S.A., K.L. Ratzlaff, and T. Kuwana, *Surface-enhanced resonance Raman spectroscopy of liquid chromatographic analytes on thin-layer chromatographic plates.* Analytical Chemistry (1990) **62**:14, 1438-1444.

100. Leopold, N. and B. Lendl, *On-column silver substrate synthesis and surface-enhanced Raman detection in capillary electrophoresis.* Analytical and Bioanalytical Chemistry (2010) **396**:6, 2341-2348.

101. Herman, K., et al., *In situ laser-induced photochemical silver substrate synthesis and sequential SERS detection in a flow cell.* Analytical and Bioanalytical Chemistry (2011) **400**:3, 815-820.

102. Dijkstra, R.J., et al., *Raman spectroscopy as a detection method for liquid-separation techniques.* TrAC Trends in Analytical Chemistry (2005) **24**:4, 304-323.

103. DeVault, G.L. and M.J. Sepaniak, *Spatially focused deposition of capillary electrophoresis effluent onto surface-enhanced Raman-active substrates for off-column spectroscopy.* Electrophoresis (2001) **22**:11, 2303-2311.

104. Nirode, W.F., et al., *On-Column Surface-Enhanced Raman Spectroscopy Detection in Capillary Electrophoresis Using Running Buffers Containing Silver Colloidal Solutions.* Analytical Chemistry (2000) **72**:8, 1866-1871.

105. Seifar, R.M., et al., *At-line coupling of capillary electrophoresis and surface-enhanced resonance Raman spectroscopy.* Journal of Separation Science (2002) **25**:13, 813-818.

106. Tran, C.D., *In situ identification of paper chromatogram spots by surface enhanced Raman scattering.* Journal of Chromatography A (1984) **292**:2, 432-438.

107. Li, D., et al., *Facile On-Site Detection of Substituted Aromatic Pollutants in Water Using Thin Layer Chromatography Combined with Surface-Enhanced Raman Spectroscopy.* Environmental Science & Technology (2011) **45**:9, 4046-4052.

108. Herman, K., et al., *In situ Silver Spot Preparation and on-Plate Surface-Enhanced Raman Scattering Detection in Thin Layer Chromatography Separation.* Journal of Applied Spectroscopy (2013) **80**:2, 311-314.

109. Horvath, E., et al., *Critical evaluation of experimental conditions influencing the surface-enhanced Raman spectroscopic (SERS) detection of substances separated by layer liquid chromatographic techniques.* Chromatographia (2000) **51**:1, S297-S301.

110. Lee, P.C. and D. Meisel, *Adsorption and surface-enhanced Raman of dyes on silver and gold sols.* The Journal of Physical Chemistry (1982) **86**:17, 3391-3395.

111. Leopold, N. and B. Lendl, *A new method for fast preparation of highly surface-enhanced Raman scattering (SERS) active silver colloids at room temperature by reduction of silver nitrate with hydroxylamine hydrochloride.* Journal of Physical Chemistry B (2003) **107**:24, 5723-5727.

112. Liu, R.M., et al., *The ultratrace detection of crystal violet using surface enhanced Raman scattering on colloidal Ag nanoparticles prepared by electrolysis.* Chinese Chemical Letters (2009) **20**:6, 711-715.

113. Kudelski, A., *Raman studies of rhodamine 6G and crystal violet sub-monolayers on electrochemically roughened silver substrates: Do dye molecules adsorb preferentially on highly SERS-active sites?* Chemical Physics Letters (2005) **414**:4–6, 271-275.

114. Dijkstra, R.J., et al., *Substrates for the at-line coupling of capillary electrophoresis and surface-enhanced Raman spectroscopy.* Analytica Chimica Acta (2004) **508**:2, 127-134.

115. Fujiyoshi, S., T. Ishibashi, and H. Onishi, *Low-frequency vibrations of molecular submonolayers detected by time-domain Raman spectroscopy.* Journal of Molecular Structure (2005) **735–736**:0, 169-177.

116. Schulz, H., M. Baranska, and R. Baranski, *Potential of NIR-FT-Raman spectroscopy in natural carotenoid analysis.* Biopolymers (2005) **77**:4, 212-221.

117.   Vogel, E., A. Gbureck, and W. Kiefer, *Vibrational spectroscopic studies on the dyes cresyl violet and coumarin 152.* Journal of Molecular Structure (2000) **550–551**:0, 177-190.

118.   Frens, G., *Controlled Nucleation for the Regulation of the Particle Size in Monodisperse Gold Suspension.* Nature Physical Science (1973) **241**:1, 20-22.

119.   Frens, G., *Particle size and sol stability in metal colloids.* Kolloid Z.u Z. Polymere (1972) **250** 736-741.

120.   Emory, Sr., W.E. Haskins, and S.M. Nie, *Direct observation of size-dependent optical enhancement in single metal nanoparticles.* Journal of the American Chemical Society (1998) **120**:31, 8009-8010.

121.   García de Abajo, F.J., *Colloquium: Light scattering by particle and hole arrays.* Reviews of Modern Physics (2007) **79**:4, 1267-1290.

122.   Koglin, E., B.J. Kip, and R.J. Meier, *Adsorption and Displacement of Melamine at the Ag/Electrolyte Interface Probed by Surface-Enhanced Raman Microprobe Spectroscopy.* The Journal of Physical Chemistry (1996) **100**:12, 5078-5089.

123.   House, P.G. and C.S. Schnitzer, *SERRS and visible extinction spectroscopy of copper chlorophyllin on silver colloids as a function of pH.* Journal of Colloid and Interface Science (2008) **318**:2, 145-151.

124.   Turkevich, J., P.C. Stevenson, and J. Hillier, *A study of the nucleation and growth processes in the synthesis of colloidal gold.* Discussions of the Faraday Society (1951) **11**:0, 55-75.

125.   Faraday, M., *The Bakerian Lecture: Experimental Relations of Gold (and Other Metals) to Light.* Philosophical Transactions of the Royal Society of London (1857) **147** 145-181.

126.   Wieser, *Inorganic Colloid Chemistry I.* 1933, New York: John Wiley and Sons.

127.   Thiessen, Z. anorg. Chemie (1929) **180** 57.

128.   Donau, Monatsh. (1905) **25** 525.

129.   Haiss, W., et al., *Determination of size and concentration of gold nanoparticles from UV-Vis spectra.* Analytical Chemistry (2007) **79**:11, 4215-4221.

130.   Boca, S.C., C. Farcău, and S. Aştilean, *The study of Raman enhancement efficiency as function of nanoparticle size and shape.* Nuclear Instruments & Methods in Physics Research Section B-Beam Interactions with Materials and Atoms (2009) **267**:2, 406-410.

131.   Takahashi, H., et al., *Surface modification of gold nanorods using layer-by-layer technique for cellular uptake.* Journal of Nanoparticle Research (2008) **10**:1, 221-228.

132.   Boca, S.C. and S. Astilean, *Detoxification of gold nanorods by conjugation with thiolated poly(ethylene glycol) and their assessment as SERS-active carriers of Raman tags.* Nanotechnology (2010) **21**:23, 235601.

133.   Kneipp, K., et al., *Single Molecule Detection Using Surface-Enhanced Raman Scattering (SERS).* Physical Review Letters (1997) **78**:9, 1667-1670.

134.   Kneipp, K., et al., *Surface-enhanced Raman scattering (SERS)—a new tool for single molecule detection and identification.* Bioimaging (1998) **6**:2, 104-110.

135.   Kneipp, J., H. Kneipp, and K. Kneipp, *SERS-a single-molecule and nanoscale tool for bioanalytics.* Chemical Society Reviews (2008) **37**:5, 1052-1060.

136.   Grüneberg, R.N., *Changes in urinary pathogens and their antibiotic sensitivities, 1971–1992.* Journal of Antimicrobial Chemotherapy (1994) **33**:suppl A, 1-8.

137.   Carmeli, Y., et al., *Health and economic outcomes of antibiotic resistance in pseudomonas aeruginosa.* Archives of Internal Medicine (1999) **159**:10, 1127-1132.

138.   Cialla, D., et al., *Surface-enhanced Raman spectroscopy (SERS): progress and trends.* Analytical and Bioanalytical Chemistry (2012) **403**:1, 27-54.

139.	Ivleva, N.P., et al., *In Situ Surface-Enhanced Raman Scattering Analysis of Biofilm.* Analytical Chemistry (2008) **80**:22, 8538-8544.

140.	Çulha, M., et al., *Characterization of Thermophilic Bacteria Using Surface-Enhanced Raman Scattering.* Appl. Spectrosc. (2008) **62**:11, 1226-1232.

141.	Kahraman, M., et al., *Convective Assembly of Bacteria for Surface-Enhanced Raman Scattering.* Langmuir (2008) **24**:3, 894-901.

142.	Walter, A., et al., *Towards a fast, high specific and reliable discrimination of bacteria on strain level by means of SERS in a microfluidic device.* Lab on a Chip (2011) **11**:6, 1013-1021.

143.	Kahraman, M., K. Keseroğlu, and M. Çulha, *On Sample Preparation for Surface-Enhanced Raman Scattering (SERS) of Bacteria and the Source of Spectral Features of the Spectra.* Appl. Spectrosc. (2011) **65**:5, 500-506.

144.	Notingher, I. and L.L. Hench, *Raman microspectroscopy: a noninvasive tool for studies of individual living cells in vitro.* Expert Review of Medical Devices (2006) **3**:2, 215-234.

145.	Lin-Vein, D., et al., *The Handbook of Infrared and Raman Characteristic Frequecies of Organic Molecules* 1991: Academic Press Limited.

146.	Sengupta, A., et al., *Bioaerosol characterization by surface-enhanced Raman spectroscopy (SERS).* Journal of Aerosol Science (2005) **36**:5–6, 651-664.